A STUDY OF THE SIMULATION OF THE FLIGHT PERFORMANCE OF CHARRING ABLATORS IN GROUND FACILITIES

A Thesis

Presented to

the Faculty of the School of Engineering and Applied Science

University of Virginia

In Partial Fulfillment

of the Requirements for the Degree

Master of Aerospace Engineering

---

by

Stephen S. Tompkins

June 1968

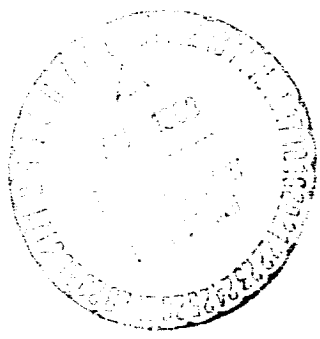

APPROVAL SHEET

This thesis is submitted in partial fulfillment of

the requirements for the degree of

Master of Aerospace Engineering

Stephen S. Tompkins
Author

Approved:

John Kenneth Haviland
Faculty Advisor

Dean, School of Engineering and
Applied Science

June 1968

ACKNOWLEDGMENTS

The author is indebted to the National Aeronautics and Space Administration for permission to use material obtained from a research project at the Langley Research Center in this thesis. Particular thanks are due Mr. Robert T. Swann for his guidance during this investigation.

The author is also grateful to Dr. John K. Haviland for his comments and suggestions in preparing this thesis.

TABLE OF CONTENTS

LIST OF TABLES

LIST OF FIGURES

FIGURE PAGE

FIGURE PAGE

SYMBOLS

a	defined by equation (7a)
C_e	oxygen concentration by weight external to boundary layer
c_p	specific heat
$\overline{c_p}$	specific heat of gaseous products of pyrolysis
D	binary diffusion coefficient
f	volatile fraction in uncharred material
Δh	heat of combustion per unit weight of char consumed
Δh_{eff}	effective heat of pyrolysis
Δh_p	heat of pyrolysis
h	total enthalpy
k	thermal conductivity
$\dot{m}_c$	rate of char loss
$\dot{m}_p$	rate of pyrolysis
N_{Le}	Lewis number
N_{Pr}	Prandtl number
N_{SC}	Schmidt number
$\vec{n}$	vector normal to surface
P	pressure
q_l	heat input to surface resulting from combustion
q_c	hot-wall convective heating rate
$q_{c,net}$	defined by equation (4)
q_{co}	cold-wall convective heating rate
q_r	radiant heating rate

Q_c	integrated convective heat input
R_b	cylindrical body radius
s	distance from stagnation point along surface
t	time
$\vec{t}$	vector tangential to surface
T	temperature
T_p	temperature of pyrolysis
W_c	char weight
W_i	initial weight
X	coordinate normal to surface
α	absorptivity of char
β	defined by equation (7c)
γ	heat transfer coefficient, equation (B-1)
ϵ	emissivity
η	transpiration coefficient
λ	weight of char removed per unit weight of oxygen
ρ	density
σ	Stefan-Boltzmann constant
τ	shear stress
ϕ	defined by equation (7b)
ψ	defined by equation (B-7)

Subscripts

D	diffusion controlled
c	char
e	external to boundary

eq	equilibrium
m	extremum
p	pyrolysis
r	reference value
s	surface value
w	condition at wall
1,2	different environments

ABSTRACT

An analytical and experimental investigation has been made to evaluate a technique by which the performance of charring ablators in high enthalpy environments can be determined by testing in low enthalpy environments. Relationships are presented which indicate that proper simulation of a high enthalpy environment can be achieved by adjusting the heat input and stream oxygen content in the low enthalpy environment.

Tests with a high and a low density phenolic nylon charring ablator were made at two enthalpy levels to validate the simulation technique. Values of the principal test parameters in the high enthalpy environment and the low enthalpy test environment were, respectively, enthalpy, 1000 and 3000 Btu/lbm, cold-wall convective heating rates, 170 and 160 Btu/ft^2 sec, stream oxygen mass fraction 0.23 and 0.05. A comparison of the ablation performance data indicates that satisfactory simulation was obtained.

Although the present tests were conducted at constant enthalpy heating, a method is outlined to extend the present technique to simulate the ablation performance at variable enthalpy in a constant enthalpy environment by step changes in oxygen concentration.

CHAPTER I

INTRODUCTION

The charring plastics have been shown to provide a practical method for protecting the interior of a spacecraft from the atmospheric heating encountered during entry into planetary atmosphere. The behavior of this type of material when subjected to heating is very complex, and extensive experimental (Refs. 1 and 2) and analytical investigations (Refs. 3, 4, 5, and 6) have been undertaken to study this problem.

Experimental studies have been conducted in a variety of test facilities which produce a wide range of environmental conditions. Many of these facilities provide the appropriate heating rate, but are characterized by low enthalpy levels. The high enthalpy facilities are usually restricted to tests of small specimens and are therefore useful only for materials evaluation tests. Some of the low enthalpy facilities can be used to test much larger specimens and combined thermal and mechanical performance can be investigated. However, ablation performance at low enthalpy levels may differ from that which would be obtained at high enthalpy levels.

In the present paper the conditions under which the performance of a charring ablator in a high enthalpy environment, typical of reentry, can be simulated in a low enthalpy test facility are examined. The results of Reference 7 are used to determine quantitative relationships between results obtained under different test conditions. Equations are presented to determine the test conditions which should be used in a

facility having a given enthalpy to produce the same material performances that would be obtained in an environment having a different enthalpy.

Experimental results for a low-density and a high-density charring ablator are presented to determine if simulation of the ablation performance was achieved.

The basic equations resulting from this study and a set of qualifying test data are presented in Reference 8. The data of Reference 8, however, are preliminary and indicate only that the overall performance can be duplicated. In the present study the complete reproduction of the transient behavior is considered as well as the overall ablation performance.

CHAPTER II

APPROXIMATE ANALYSIS OF CHARRING ABLATORS

An analytical model of the charring ablator is presented in Reference 3. This model is shown schematically in Figure 1. The outer surface of the char layer is subjected to aerodynamic heating. As the material is heated, the material undergoes degradation, forming a char layer which provides both insulation and a high-temperature outer surface for reradiation. The heat passing through this layer is partially absorbed by pyrolysis at the interface between the char layer and the uncharred material, and the remaining heat is conducted into the uncharred material. The gases generated by pyrolysis transpire through the char layer and are injected into the boundary layer. The gases are heated as they pass through the char, which reduces the quantity of heat conducted to the pyrolysis interface. When these gases are injected into the boundary layer, the convective heat transfer is reduced. In addition to the gases produced by pyrolysis, a residue remains at the interface and adds to the thickness of the char layer. At the same time, char removal may occur as a result of thermal, chemical, or mechanical process. Thus the total char thickness may increase or decrease depending on the relative rates of formation and removal of the char. These processes are related quantitatively in the following section.

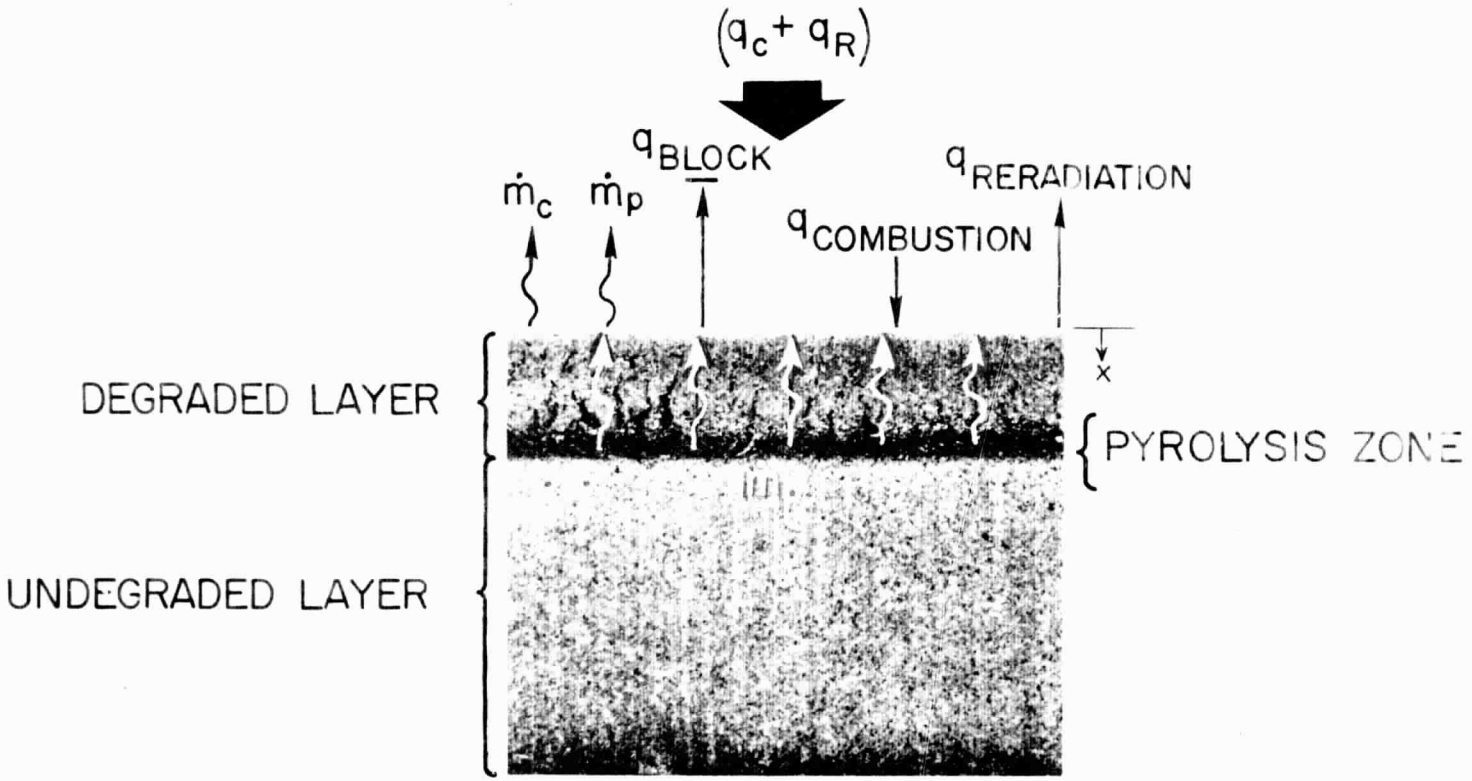

Figure 1.- Schematic diagram of charring ablator.

Governing Equations

It is assumed that thermal properties of the char are functions only of temperature, that all heat flow is normal to the surface, and that gases transpiring through the char are at the same temperature as the char. The differential equation governing the temperature in the char is (from Ref. 3),

$$\frac{\partial}{\partial X}\left(k \frac{\partial T}{\partial X}\right) + \dot{m}_p \overline{c_p} \frac{\partial T}{\partial X} = \rho c_p \frac{\partial T}{\partial t} \tag{1}$$

To solve this equation, conditions on the temperature or heat flux and mass transfer must be given at each boundary. In a charring ablator with low rates of mass transfer into the boundary layer and with char removal by oxidation only, the conditions at the char surface are as follows (Ref. 3),

$$\underbrace{q_{c,net} + \alpha q_r + \dot{m}_c \Delta h_c}_{\text{Heat input}} = \underbrace{\sigma \epsilon T^4}_{\text{Reradiation}} - \underbrace{k \frac{\partial T}{\partial X}}_{\text{Conducted to interior}} \tag{2}$$

where, for diffusion controlled oxidation with a Lewis number of 1,

$$\dot{m}_c = \lambda C_e \frac{q_{c,net}}{(h_e - h_w)} \tag{3}$$

and

$$q_{c,net} = q_{co}\left(1 - \frac{h_w}{h_e}\right)\left[1 - (\eta_c \dot{m}_c + \eta_p \dot{m}_p)\frac{h_e}{q_{co}}\right] \tag{4}$$

Pyrolysis occurs in a zone between the char and the uncharred material. In many cases this zone is very thin and can be treated as a plane. Reference 9 indicates that treating the pyrolysis zone as a plane is a reasonable assumption. In this case, the temperature of the char and the uncharred material must be the same at the pyrolysis plane and, in general, this temperature will be a function of the rate of pyrolysis,

$$T_{char} = T_{uncharred} = F(\dot{m}_p)$$

From an energy balance at the pyrolysis plane,

$$-\left(k \frac{\partial T}{\partial X}\right)_{char} = \dot{m}_p \Delta h_p - \left(k \frac{\partial T}{\partial X}\right)_{uncharred} \tag{5}$$

Solution of the above equations, together with the transient heat conduction equation in the uncharred material, provides an estimate for all aspects of the performance of a thermal protection system based on a charring ablator. Detailed application of these equations is presented in Reference 3.

Approximate Equations

An approximate analysis of the performance of charring ablators is presented in Reference 7. The analysis is based on a number of simplifying assumptions. These assumptions are discussed in Appendix A. The analysis provides equations for calculating the amount of material degraded by heating at any time. The char thickness and the amount of

char removed can also be determined. However, the internal temperatures cannot be determined on the basis of such a simplified analysis.

For the case when enthalpy, $\frac{q_r}{q_{co}}$, and stream oxygen concentration are constant and the oxidation process is diffusion controlled, the weight of char accumulated for the convective heat input, Q_c, is (from Ref. 7),

$$\frac{W_i - W_c}{W_{c,m}} - \left(1 + \frac{\phi\beta}{W_{c,m}}\right)\ln\left(\frac{1 - \frac{W_c}{W_{c,m}}}{1 - \frac{W_i}{W_{c,m}}}\right) = \frac{a}{1 + a\eta}\,\frac{Q_c}{(h_e - h_w)W_{c,m}} \tag{6}$$

where

$$a = C_e\lambda \tag{7a}$$

$$\phi = \frac{1 + \eta(a\Delta h + h_e - h_w)}{\Delta h_{eff}(1 + a\eta)} \tag{7b}$$

$$\beta = \frac{k_r\rho}{\sigma\epsilon(T_r^2 + T_p^2)(T_r + T_p)} \tag{7c}$$

and

$$W_{c,m} = \beta\left[\left(\frac{\Delta h}{\Delta h_{eff}} + \frac{h_e - h_w}{a\Delta h_{eff}}\right)\frac{1 - f}{f} + \frac{\alpha q_r}{q_{co}}\,\frac{(h_e - h_w)}{\Delta h_{eff}}\left(\frac{1 - f + a\eta}{af}\right) - 1\right] \tag{8}$$

The extremum char weight, $W_{c,m}$, is the weight of char which would accumulate if a specimen of infinite thickness was heated indefinitely at a given heating rate.

The amount of material pyrolyzed is (Ref. 7),

$$W_p = \frac{W_c - W_i + \left(\frac{a}{1 + a\eta}\right)\frac{Q_c}{(h_e - h_w)}}{\frac{1 - f + a\eta}{f(1 + a\eta)}} \tag{9}$$

and the total weight of material degraded is

$$W = \frac{W_c - W_i + \left(\frac{a}{1 + a\eta}\right)\frac{Q_c}{(h_e - h_w)}}{\frac{1 - f + a\eta}{(1 + a\eta)}} + W_i \tag{10}$$

CHAPTER III

SIMULATION OF ABLATION PERFORMANCE

The equations presented in the previous section can be used to determine the performance of charring ablators exposed to various thermal environments with constant enthalpy. In this section, the conditions under which the same ablation performance can be obtained in different but constant enthalpy heating environments will be investigated. Relationships are determined that specify the required environment for simulation.

It is assumed that the enthalpy level of the test stream is relatively constant and much lower than the stream in which the performance is to be determined. This is the characteristic situation which is encountered when an attempt is made to evaluate reentry performance using large-scale specimens.

An examination of the equations in the previous section shows that environmental parameters affect performance directly only at the heated surface. Therefore, any two environments so related that the inputs at the surface are the same should result in the same ablation performance of the material. That is, if the surface has a given history of location and temperature, all phenomena beneath the surface are independent of the particular environment which produces the surface conditions.

The aerodynamic inputs to an ablating surface may be classified as thermal, chemical, and mechanical, and represented analytically as follows:

Thermal

$$\alpha q_r + q_{c,net} \tag{11a}$$

Chemical

$$\dot{m}(O_2) \tag{11b}$$

Mechanical

$$P_w\vec{n} + \tau_w\vec{t} \tag{11c}$$

Only oxidation is considered here under chemical inputs. In some cases, stream species other than oxygen may interact with the surface, but the following procedure can be extended directly to such cases and they will not be considered here.

No satisfactory general theory of the effects of mechanical inputs on the performance of charring ablators is available. However, experimental data indicate that at low shear stress levels, such stress has no effect on thermal performance and can be neglected.

Both convective and radiative heating can exist in the environments considered here. Either convection or radiation is the mode of heat transfer in most low enthalpy test facilities. The present discussion will be limited to the case where convective heating only is present in the low enthalpy environment, and both convection and

radiation may exist at the high enthalpy environment. Appendix B discusses the case when radiation is the prime mode of heat transfer in the low enthalpy environment.

Two conditions that should exist to obtain simulation are:

$$(W_c)_1 = (W_c)_2 \quad \text{and} \quad (W_{c,m})_1 = (W_{c,m})_2 \tag{12}$$

The ablation performance in environment 2 is to be simulated in environment 1. Assuming convective heating to be the only mode of heat transfer in environment 1 and equating the extremum char weights, equation (8), for the two environments,

$$\left\{\beta\left[\left(\frac{\Delta h}{\Delta h_{eff}} + \frac{h_e - h_w}{a\Delta h_{eff}}\right)\frac{1-f}{f} - 1\right]\right\}_1 = \left\{\beta\left[\left(\frac{\Delta h}{\Delta h_{eff}} + \frac{h_e - h_w}{a\Delta h_{eff}}\right)\frac{1-f}{f} - 1\right]\right\}_2 \tag{13}$$

Since the material properties in equation (13) are considered invariant with respect to the environment, equation (13) simplifies to

$$\left(\frac{C_e}{h_e - h_w}\right)_1 = \left(\frac{C_e}{h_e - h_w}\right)_2 \left[1 + \frac{\alpha q_r}{q_{co}} \frac{(1 - f + a\eta)}{1 - f}\right]_2^{-1} \tag{14}$$

The material and the environment interact directly only at the interface between them. Therefore, the net aerodynamic heat input should be the same in the two conditions, that is,

$$(q_{c,net})_1 = (q_{c,net} + \alpha q_r)_2 \tag{15}$$

To obtain the heat input needed for simulation, equation (6) is first used to calculate the char weight W_{c_2} produced in environment 2 for a given convective heat input. This char weight, W_{c_2}, which equals W_{c_1}, and the known environmental parameters of the first environment are then used in equation (6) to determine the convective heat input required in environment 1 to obtain simulation.

Because of the transcendental character of equation (6), equations (6) and (10) cannot be solved explicitly to obtain a direct relation between weight of material degraded and heat input. Therefore, it was found advantageous to solve these equations for the required simulation test conditions, as well as char weight and weight of material degraded, on a digital computer.

To summarize, the following procedure may be used to obtain the test conditions required to simulate, in a known constant enthalpy ground test environment, the ablation performance of a charring ablation in a different but constant enthalpy environment:

1. Equation (14) relates the oxygen concentrations of the two environments each of different but known enthalpies.

2. The convective heat input required for simulation is obtained by using equation (6) to determine the char weight produced by the second environment; then by utilizing the identity in equation (12) and all of the known environmental parameters, equation (6) is solved for the heat input for the ground test.

The weight of char formed, equation (6), and the weight of material degraded, equation (10), depend on an integrated heat input and are independent of the heating rate history. Therefore, for tests to evaluate degradation characteristics, test time is related to flight time, through equation (15),

$$t_1 = \frac{\int_o^{t_2} (q_{c,net} + \alpha q_r)_2 \, dt}{(q_{c,net})_1} \tag{16}$$

To reproduce transient effects, however, test times must be the same.

CHAPTER IV

TEST SPECIMENS

Materials

Two char forming ablation materials were used in this investigation. One material contained, by weight, 50-percent powered nylon and 50-percent powered phenolic resin and was pressure molded to a density of 75 lb/ft^3. The other material contained, by weight, 40-percent powered nylon, 37-percent powered phenolic resin, and 23-percent phenolic microspheres, and was pressure molded to a density of 34 lb/ft^3. These materials represent two types of ablation materials that have been extensively tested. The low-density material is representative of a group of materials that have been flight tested and have application to future spacecraft.

The thermophysical properties for these materials, required by the present analysis, are given in Table I. These properties were obtained from Reference 10 and unpublished data. The thermal transport parameter, β, as defined by equation (7c), was evaluated for the present study using a reference temperature equal to the radiation equilibrium temperature based on the nominal test conditions, that is,

$$T_r = \left(\frac{q_{co}}{\sigma\epsilon}\right)^{1/4}$$

TABLE I.- MATERIAL PROPERTIES

Material property	Low-density phenolic nylon	High-density phenolic nylon
β, lbm/ft^2	0.115	0.19
Δh, Btu/lbm	5,000	5,000
λ	0.75	0.75
f	0.53	0.6
Δh_{eff}, Btu/lbm	4,340	4,340
η	0.6	0.6
ϵ	0.9	0.9
k_r, Btu/ft-sec-$^\circ$R	3.61×10^{-4}	3.19×10^{-4}
ρ, lbm/ft^3	16	30

The reference conductivity for each material was obtained with the relationship,

$$k_r = \frac{\int_{T_p}^{T_r} k \, dT}{(T_r - T_p)}$$

where k is the temperature dependent char conductivity for the respective material from Reference 10.

Geometry

The test specimens consisted of 2.5-inch-diameter cylinder, with a 4.7-inch radius spherical face, 1.25 inches thick, machined from large blanks of the phenolic nylon materials. The specimen geometry provides uniform heating and pressure across the front surface (Figs. 2 and 3).

These cylinders were bonded to bakelite holders (Fig. 2). There were eight specimens of each material, two of which contained 1-inch-diameter instrumented plugs.

Each plug contained four No. 36 chromel-alumel thermocouples (Fig. 3). The thermocouple junctions were located nominally at 0.124, 0.25, 0.375, and 0.5 inch from the front surface. The thermocouple installation recommended in Reference 11 was used. The actual thermocouple bead locations were determined by X-ray and are noted on the corresponding temperature histories.

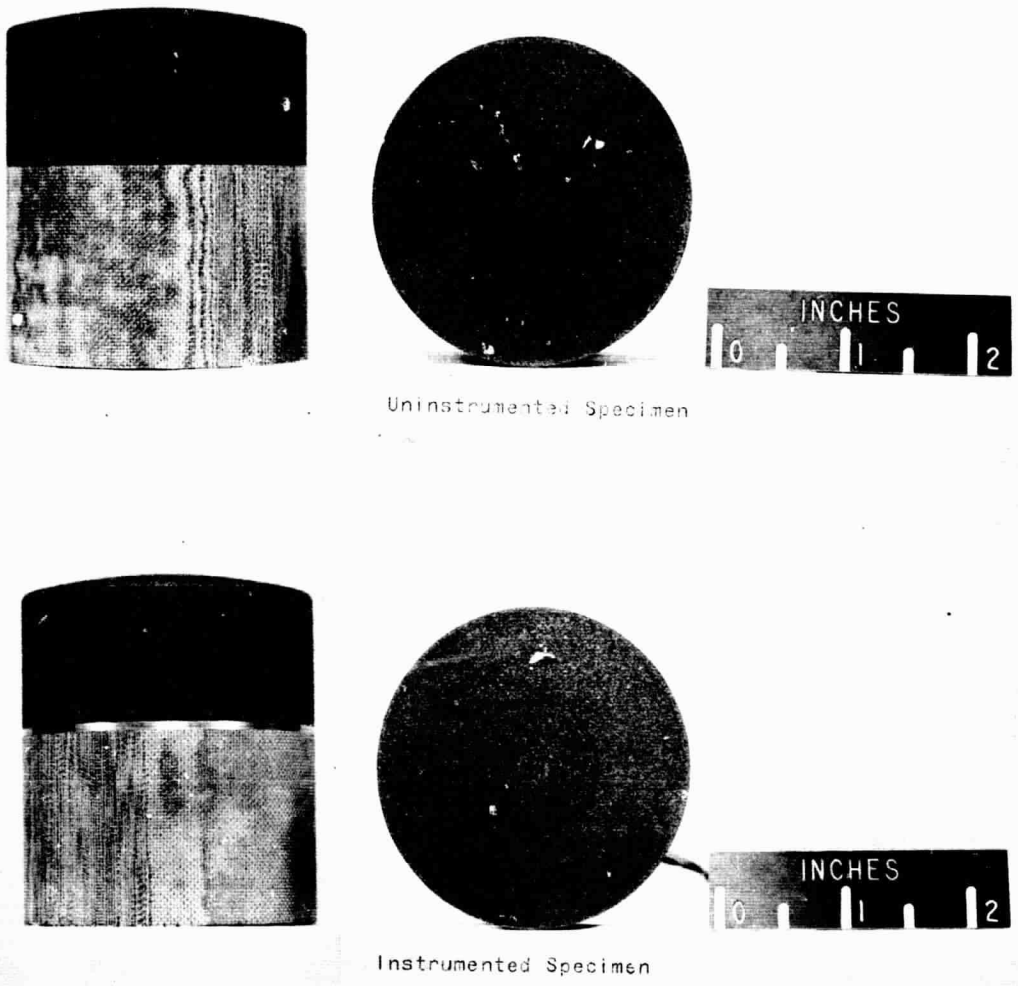

(a) Low-density phenolic nylon.

Figure 2.- Typical specimens before testing.

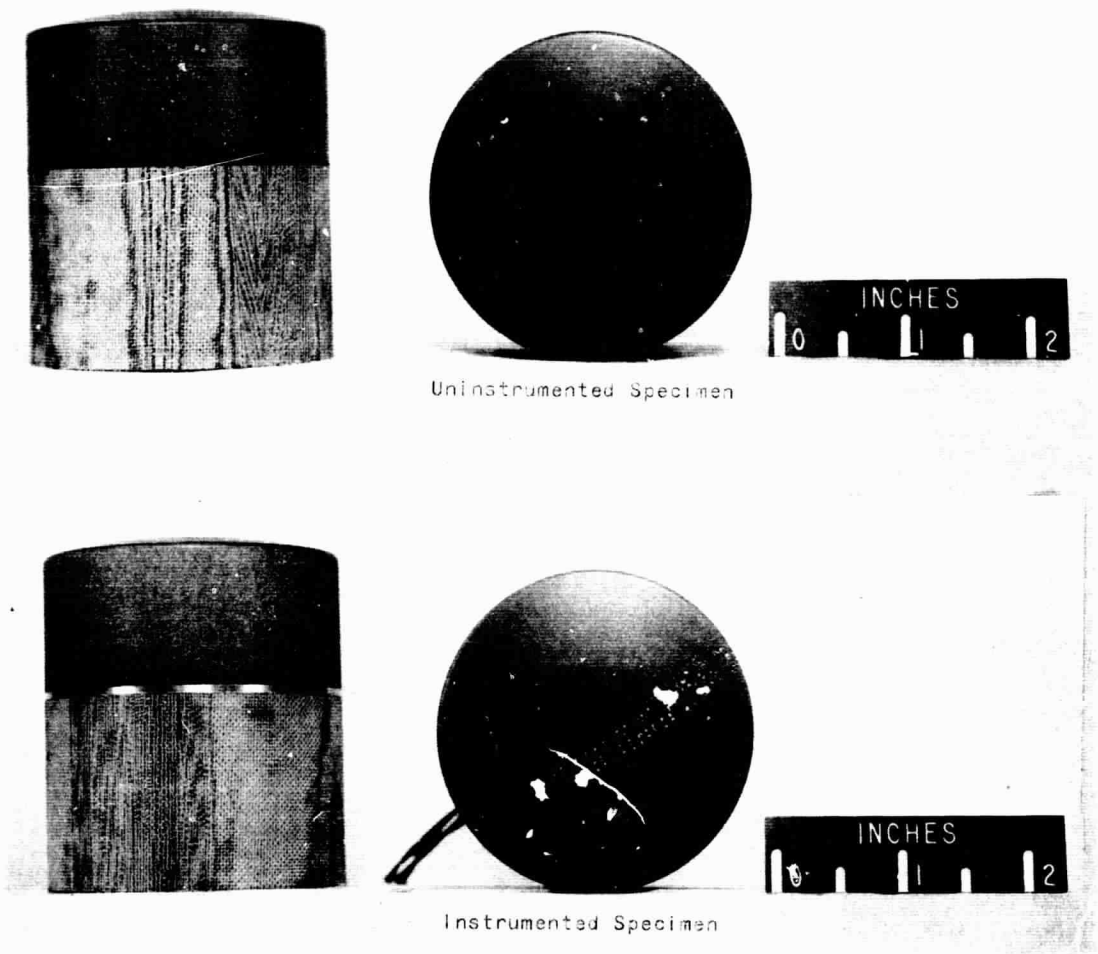

(b) High-density phenolic nylon.

Figure 2.- Concluded.

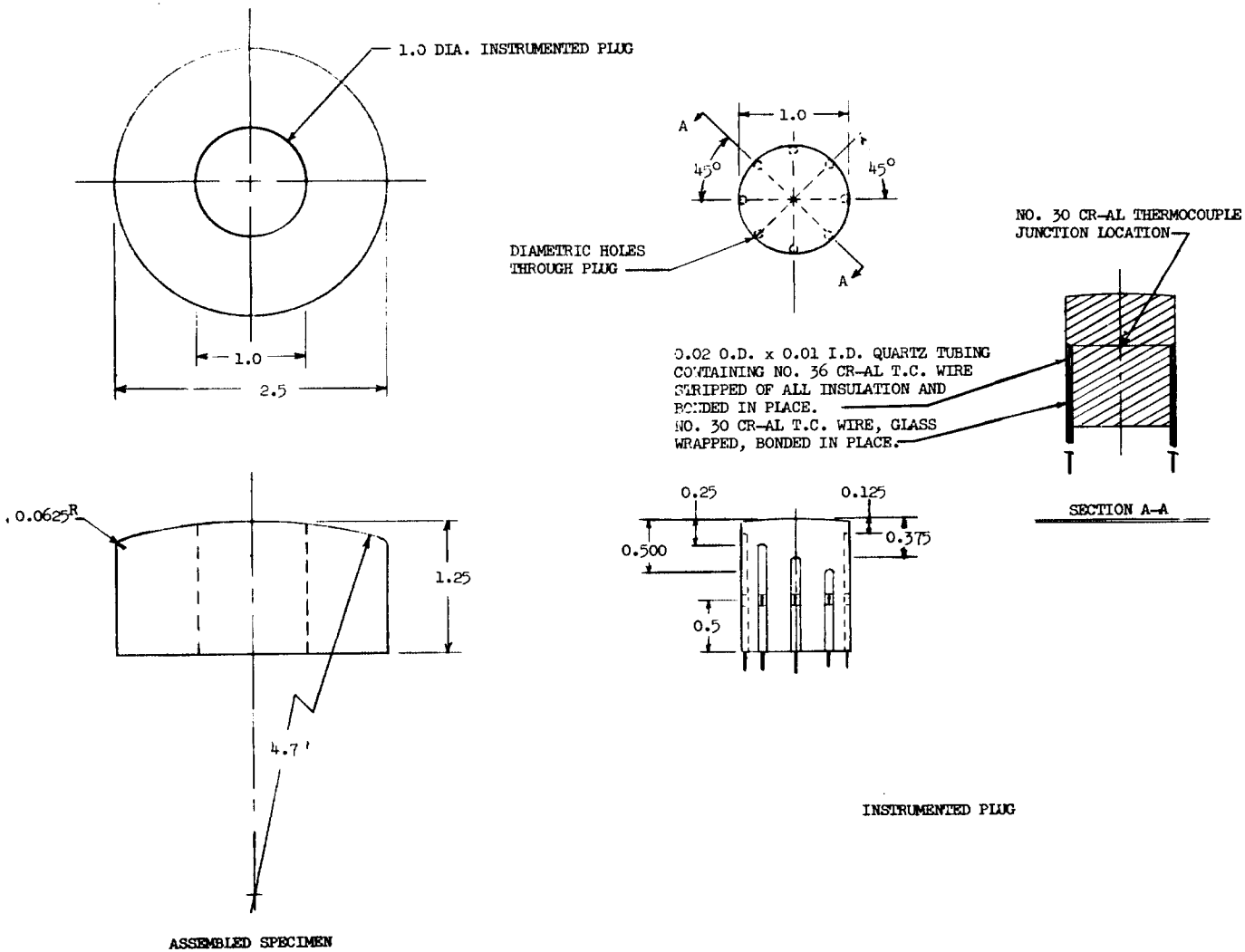

Figure 3.- Schematic of typical instrumented specimen.

CHAPTER V

TEST CONDITIONS AND PROCEDURES

Test Facilities

The 2-inch supersonic arc tunnel at the Langley Research Center was used for the tests conducted at the low enthalpy conditions. This facility is described in Reference 12. A conical nozzle with a throat diameter of 1.5 inches and an exit diameter of 4 inches was used. The desired stream oxygen concentrations are obtained by mixing air and nitrogen.

The high enthalpy direct current plasma generator at the Langley Research Center was used for the tests conducted at the high enthalpy conditions. This facility is described for a subsonic configuration in Reference 12. For the present study the facility was operated in a supersonic configuration with a 1-inch-diameter minimum and a 4-inch-diameter exit. Stream oxygen concentrations were obtained by mixing oxygen and nitrogen.

Test Conditions

The nominal test conditions for the environments were as follows:

Total enthalpy, Btu/lbm	3,000	10,000
Free-stream Mach number	3	3
Model stagnation pressure, atm	0.37	0.04
Stagnation heat-transfer rate, Btu/ft^2-sec	140	155
Free-stream oxygen content, percent	6	23
Model test time, sec	varied	varied

These test conditions were determined in the following manner. The high enthalpy test condition was established first by calibration tests using the pressure and heating rate probes of the same size and shape as the specimen. Then assuming an enthalpy of 3,000 Btu/lbm, the corresponding heat input and stream chemical composition required for simulation were determined using equations (6) and (14) and the inputs given in Table I. Convective heating was the only mode of heat transfer present in these two environments. The hot-wall enthalpy used in these calculations was based on the radiation equilibrium temperature for the test condition being considered, that is,

$$T_{eq} = \left(\frac{q_{co}}{\sigma\epsilon}\right)^{1/4}$$

Models were tested for 30, 60, 90, and 120 seconds. The instrumented models used to determine transients simulation were tested for 120 seconds. Therefore, each model tested at the high enthalpy condition for a given time had a corresponding model tested at the prescribed low enthalpy condition for the same length of time.

The present analysis is restricted to char mass loss by diffusion controlled oxidation only. Therefore, it was necessary to establish the oxidation regime the present tests would provide. The detailed ablation analysis of Reference 3 was used to compute the ratio of the char mass loss rate to the diffusion controlled mass loss rate as a function of cold-wall convective heat rate. The results of these calculations are shown in Figure 4. As can be seen, the present tests,

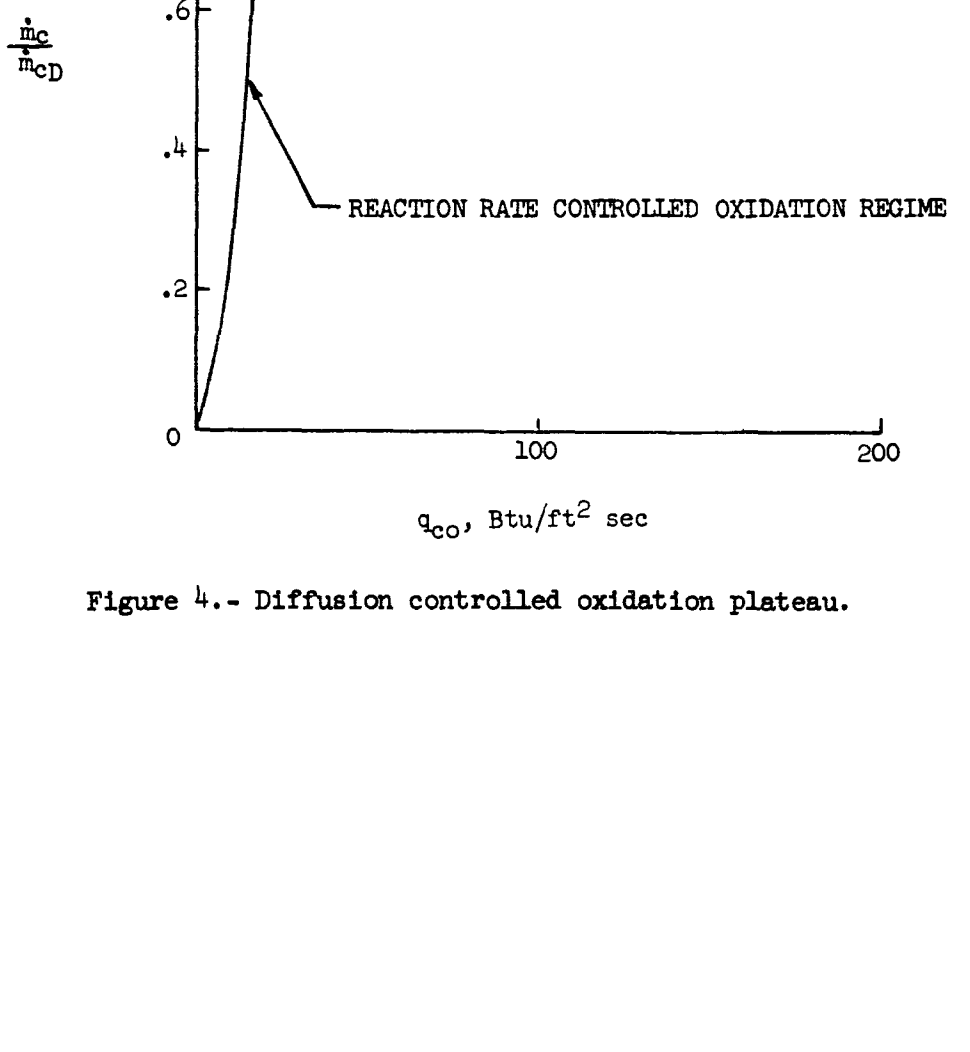

Figure 4.- Diffusion controlled oxidation plateau.

with a nominal cold-wall heating rate of 150 Btu/ft^2-sec, will provide a diffusion controlled oxidation regime.

Pressure distribution.- Stagnation pressures and pressure distributions were made on a pressure model (Fig. 5(a)) having the same external shape as the test models (Fig. 3). The pressure distributions over the model in both facilities are shown in Figure 5(b). The same distribution was obtained in both test streams. Stagnation-pressure measurements were obtained before and after each model was tested. These pressures were measured with an accuracy of ±10 percent.

Heating rate.- Stagnation heating rates and heating rate distributions were measured with an 0.032-inch-thick inconel calorimeter model (Fig. 6(a)) having the same exterior shape and dimensions as the test models (Fig. 3). The heating rate distributions over the model in both facilities were essentially the same (Fig. 6(b)). Figure 6(b) shows that the heating rate over the 1-inch-diameter instrumented plug was essentially constant. This would provide one-dimensional heating in the region on the test models where measurements were made. The measured heating rates are believed to be within ±10 percent of the actual heating rates.

Enthalpy.- Total enthalpy of the test streams was determined using References 13 and 14 and the measured stagnation pressure and heating rate for each model. The enthalpies are given in Table II for each model. The accuracy of these values is ±10 to 20 percent due to the dependence of the value on the heating rate and pressure.

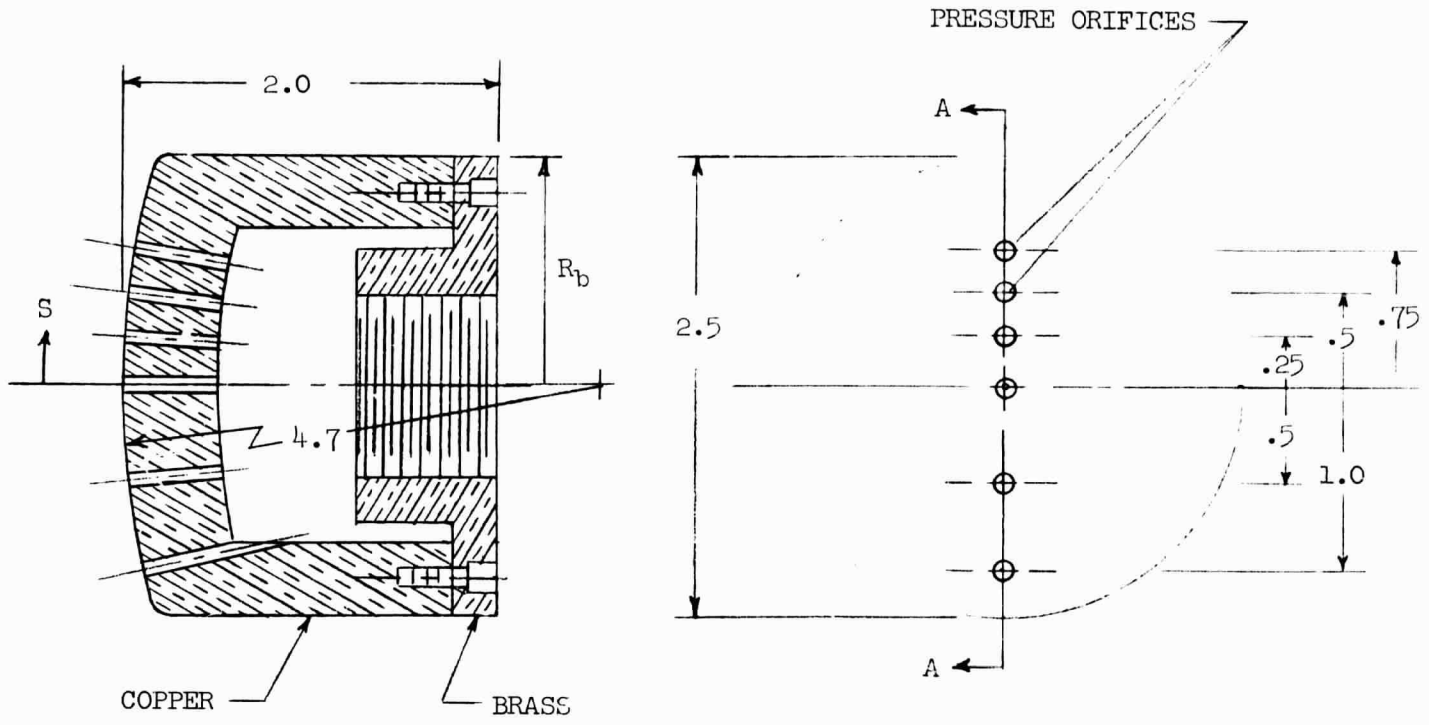

(a) Pressure probe.

Figure 5.- Pressure probe and pressure distribution.

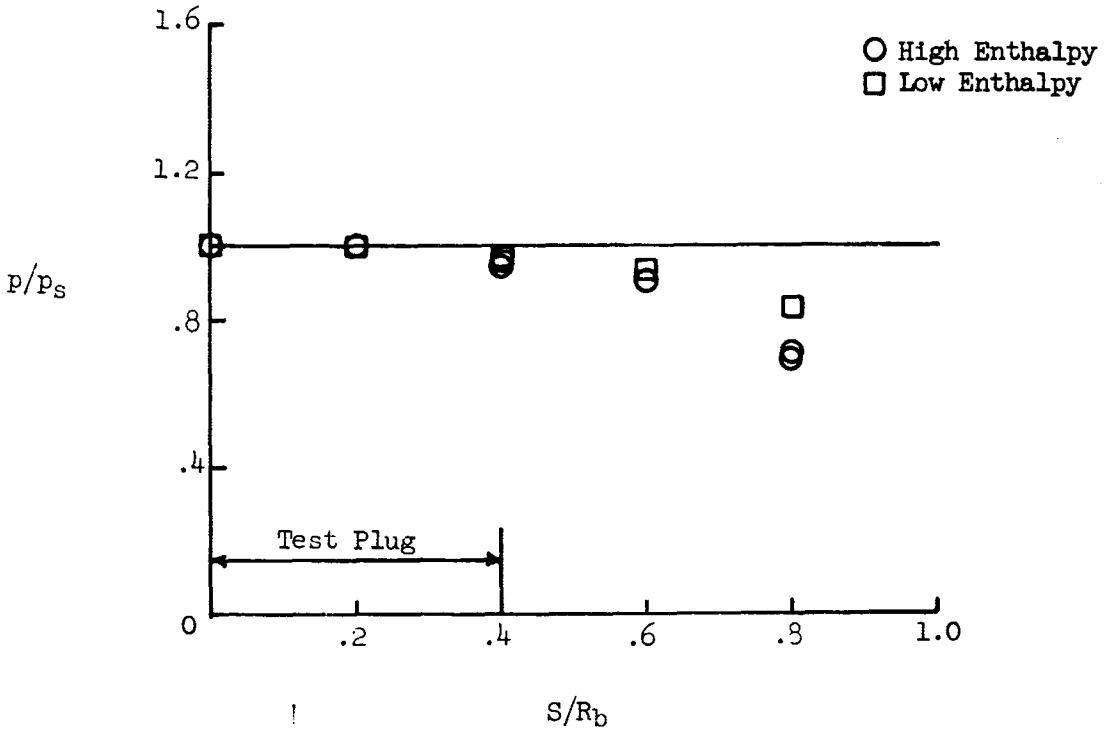

(b) Pressure distribution.

Figure 5.- Concluded.

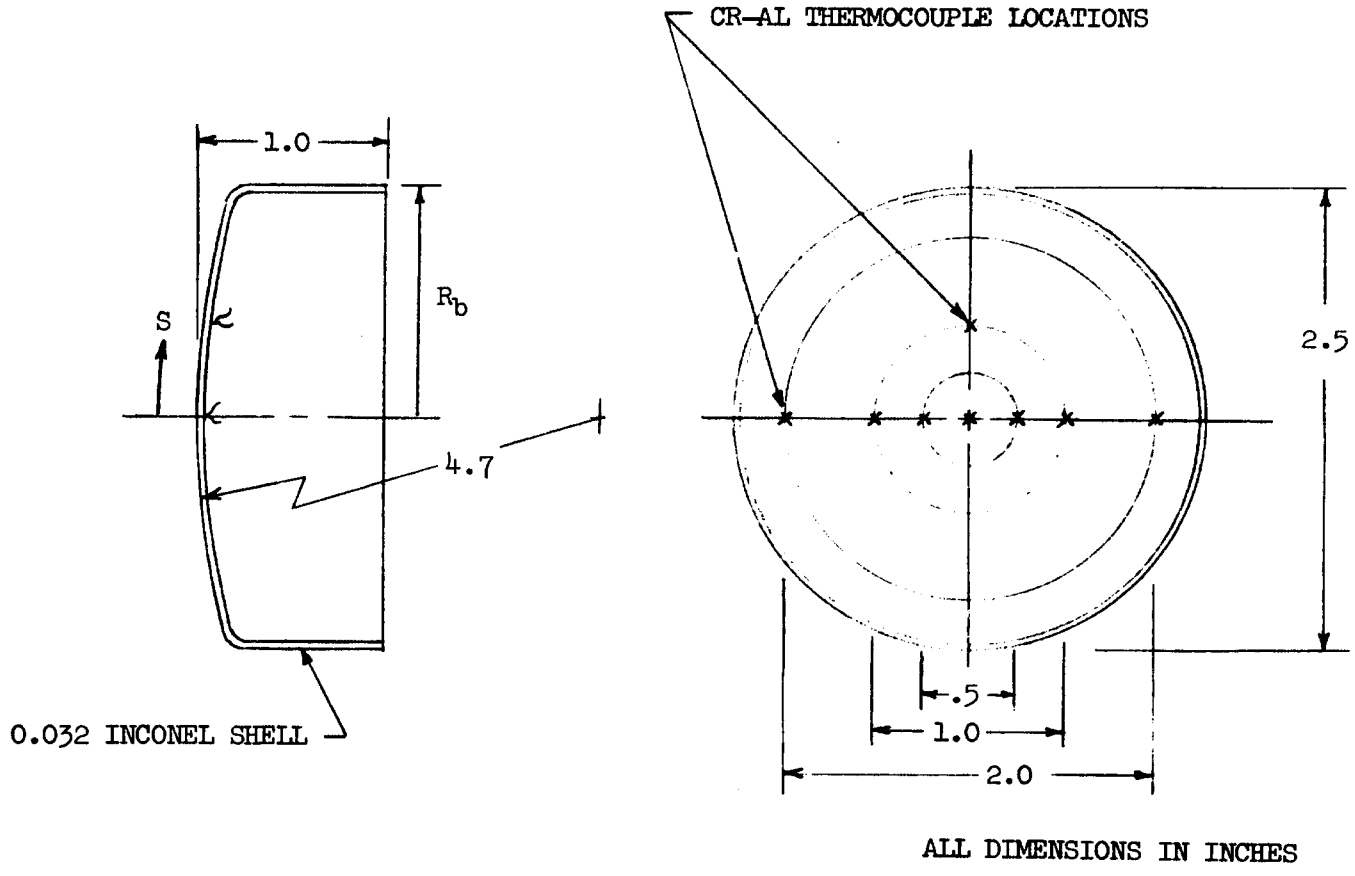

(a) Heat transfer rate probe.

Figure 6.- Heat transfer rate probe and heating rate distribution.

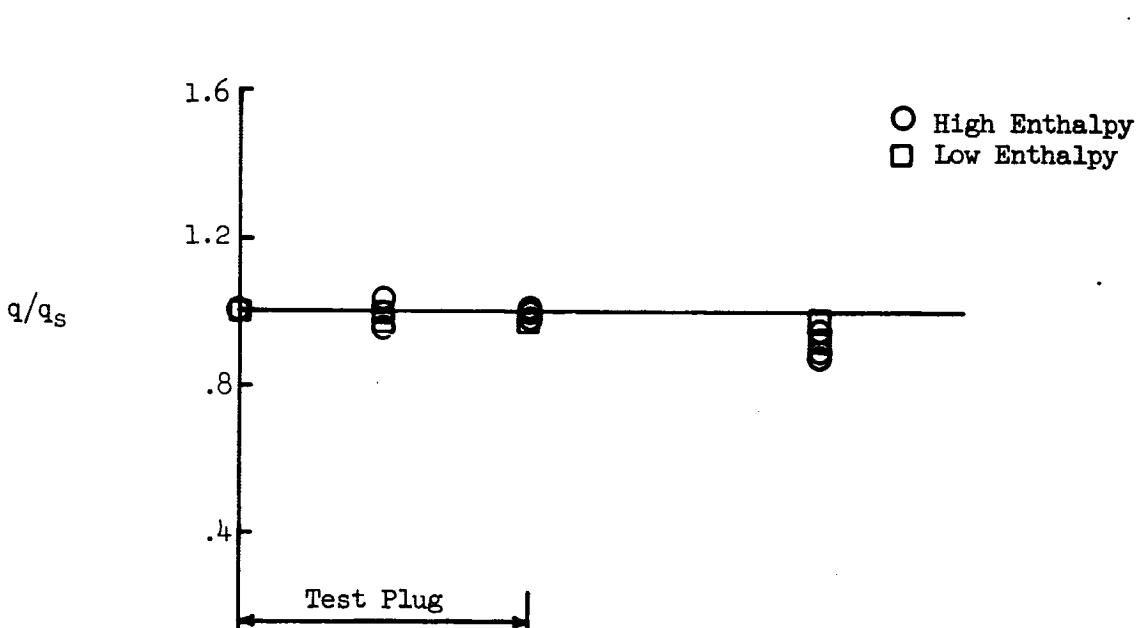

(b) Heating rate distribution.

Figure 6.- Concluded.

Test Procedure

For each test, the facility operating conditions determined from previous calibration tests were established. Heating rate and pressure measurements were made prior to and after the model was exposed to the test stream for a predetermined time. Periodic checks were made on the test conditions and adjustments were made as required. All temperature and pressure data were recorded by the Langley control digital data recording facility.

CHAPTER VI

RESULTS AND DISCUSSION

Eight pairs of specimens were tested in low and high enthalpy environments related through equations (6) and (14). Both specimens of a pair were tested for the same length of time. Four of the pairs of specimens were made of a low-density phenolic nylon material, each specimen has a LD prefix to the specimen number, and four pairs were made of a high-density phenolic nylon material, each specimen has an HD prefix to the specimen number. The test data are tabulated in Table II. All thickness measurements were made with an accuracy of ±0.01 inch.

Low-Density Phenolic Nylon Specimens

Photographs of the tested specimens are shown in Figure 7. For each specimen tested at high enthalpy there is a corresponding specimen tested at low enthalpy. The total recession, char thickness, and thickness of material degraded for each specimen are given in Table II and the data are plotted in Figure 8. Also shown in Table II are the required test conditions at low enthalpy specified by the present analysis and the actual test conditions. As can be seen the actual test conditions were very close to the required test conditions.

From a visual comparison of the paired specimens in Figure 7, it is seen that the char surface, thickness, and char structure are similar. The cracked pattern visible on the surface of each specimen is believed

TABLE II.- SUMMARY OF TEST DATA

Specimen No.	$\dot{q}$, Btu/ft^2-sec required	$\dot{q}$, Btu/ft^2-sec actual	h_e, Btu/lbm	C_e, percent required	C_e, percent actual	Test time, sec	Thickness change, in.	Char thickness, in.	Thickness of degraded material, in.
LD-15		173	11,000		24	30	0.04	0.13	0.17
14	145	162	3,500	5.8	5.8	30	0.03	0.14	0.17
13		180	12,000		24	60	0.11	0.2	0.31
7	158	157	3,400	5.1	5.8	60	0.11	0.2	0.31
16		172	10,000		32	90	0.19	0.22	0.41
5(a)	163	164	3,500	8.6	5.8	90	0.19	0.23	0.42
3(a)		175	13,000		23	120	0.29	0.23	0.52
1(a)	170	164	3,500	4.6	5.8	120	0.28	0.21	0.49
HD-10		161	9,000		24	30	0.01	0.07	0.08
9	138	159	3,600	7.6	5.8	30	0.02	0.08	0.10
8		160	9,000		24	60	0.05	0.12	0.17
7	144	165	3,500	7.3	5.5	60	0.06	0.12	0.18
13		160	10,000		26	90	0.07	0.16	0.23
11	145	160	3,600	7.3	5.8	90	0.08	0.17	0.25
3(a)		172	11,000		31	130	0.15	0.19	0.33
6(a)	150	167	3,500	7.5	5.8	121	0.14	0.2	0.34

(a) Instrumented specimens

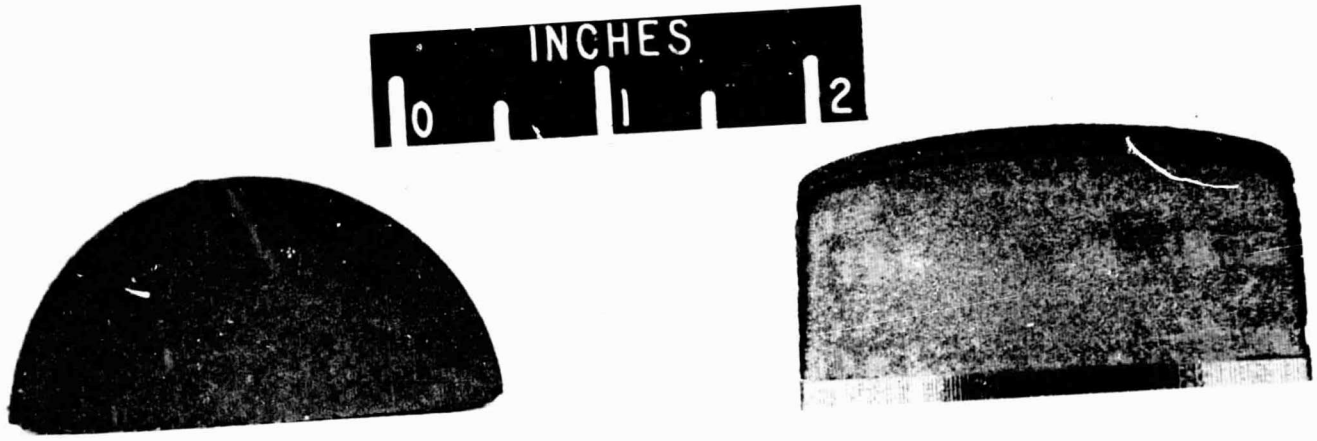

(a) Specimen LD-15 tested 30 seconds at high enthalpy.

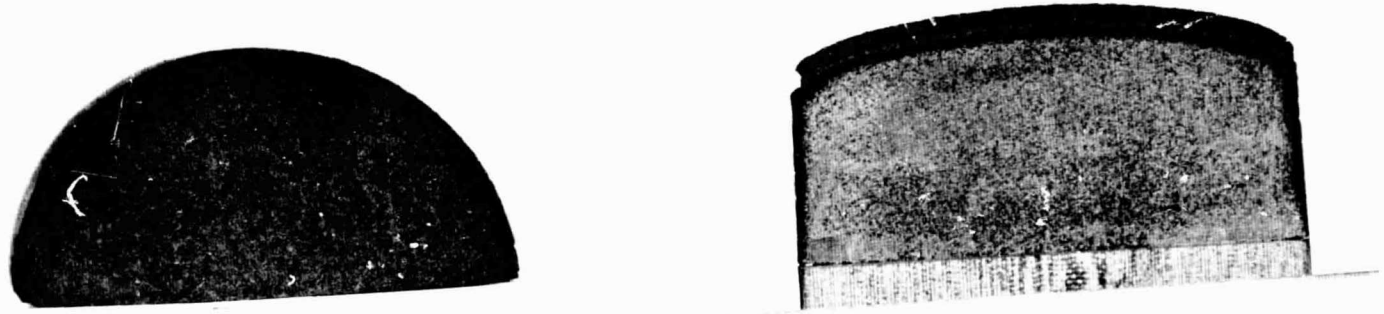

(b) Specimen LD-14 tested 30 seconds at low enthalpy.

Figure 7.- Low-density phenolic nylon after testing.

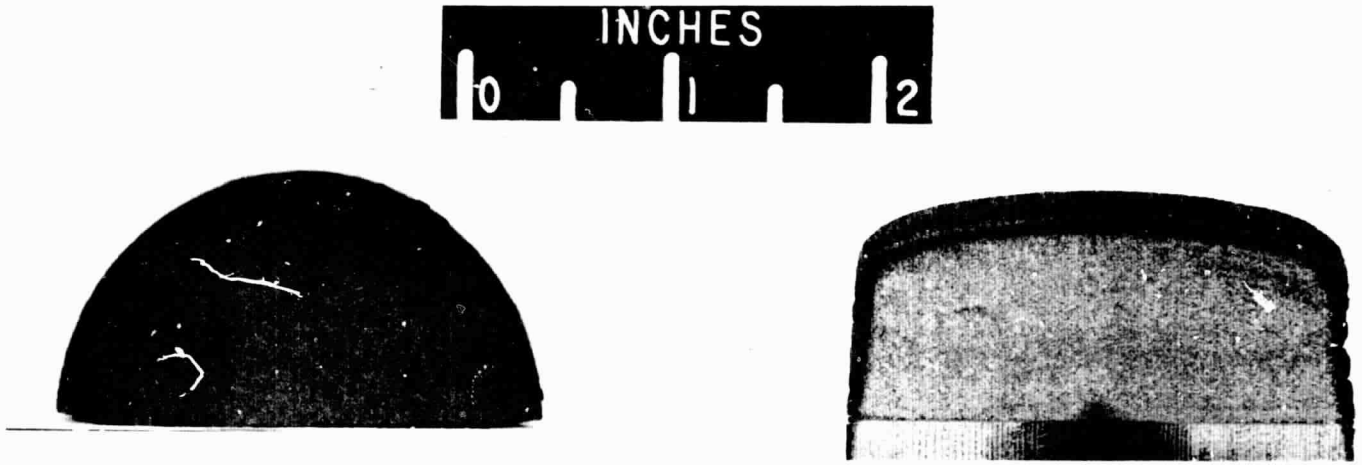

(c) Specimen LD-13 tested 60 seconds at high enthalpy.

(d) Specimen LD-7 tested 60 seconds at low enthalpy.

Figure 7.- Continued.

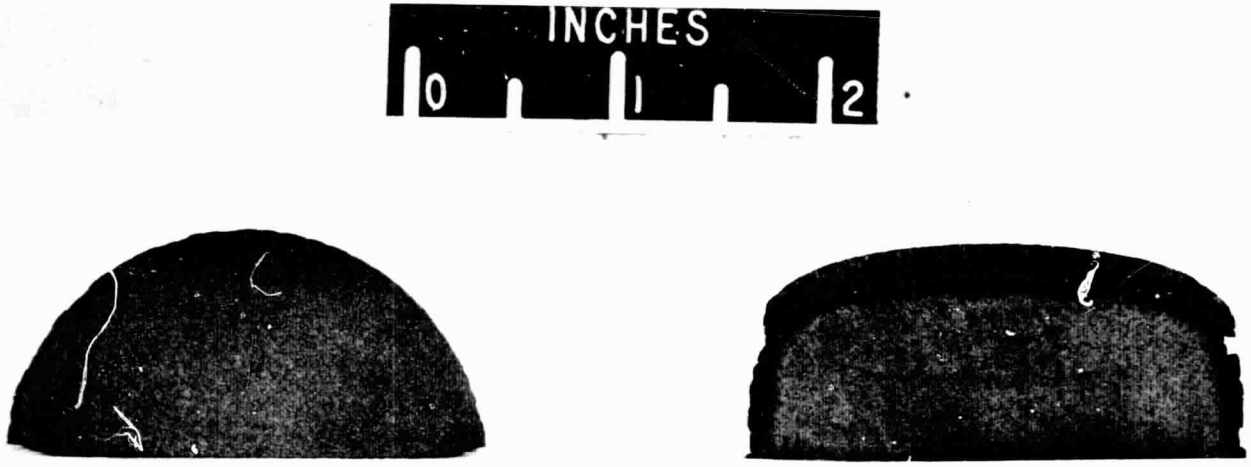

(e) Specimen LD-16 tested 90 seconds at high enthalpy.

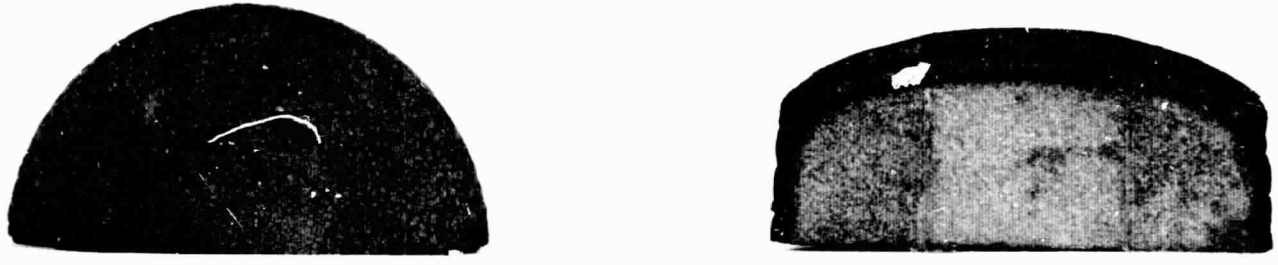

(f) Specimen LD-5 tested 90 seconds at low enthalpy.

Figure 7.- Continued.

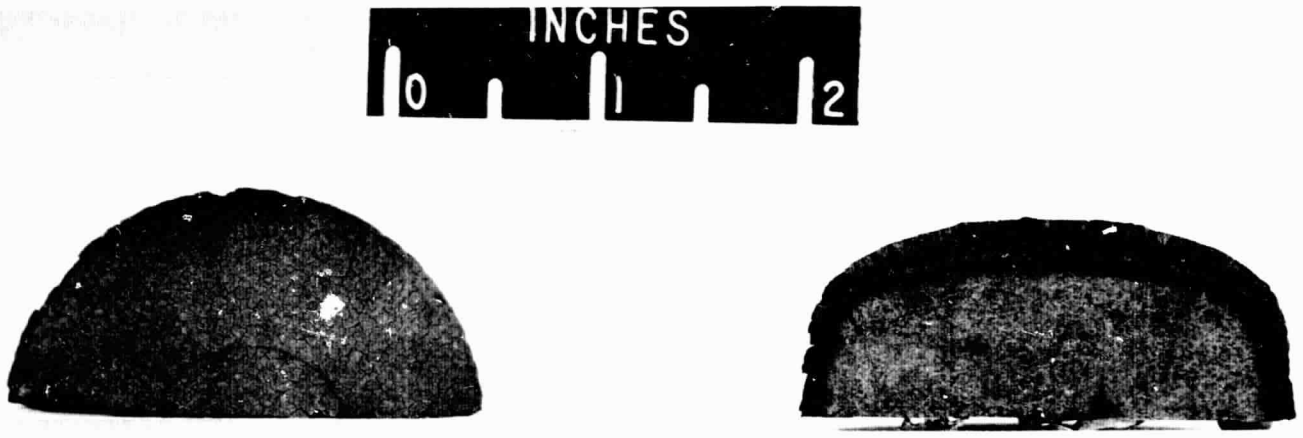

(g) Specimen LD-3 tested 120 seconds at high enthalpy.

(h) Specimen LD-1 tested 120 seconds at low enthalpy.

Figure 7.- Concluded.

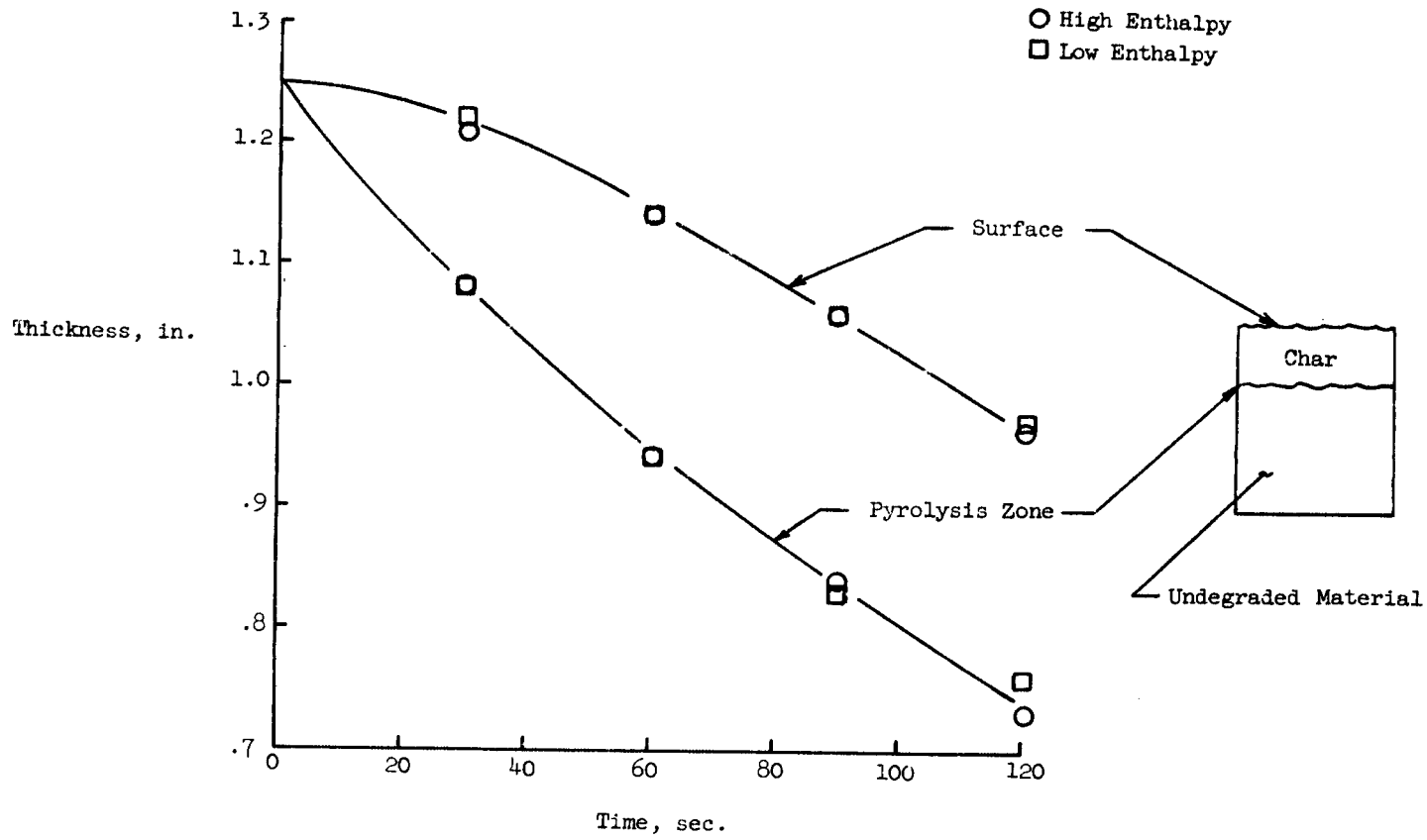

Figure 8.- Surface and interface location histories for low-density phenolic nylon specimens.

to be formed during specimen cooling. Motion pictures taken during testing do not show this pattern in either environment.

The surface recession, char thickness, and material degraded thickness data from Table II are plotted in Figure 8 as a function of time. The agreement between these thicknesses for each pair of specimens is considered satisfactory since the difference is within the accuracy of the measurements, ±0.01 inch. Figure 8, therefore, indicates that the same ablation performance was obtained in the two related environments.

Further indication of the simulation of the ablation performance can be obtained from a comparison of the internal temperature histories. Figure 9 is a comparison between the internal temperatures of a model tested in the high enthalpy environment and the low enthalpy environment. As can be seen, the agreement is very good.

An examination of the data presented in Figures 7, 8, and 9 shows that the transient ablation performance in a high constant enthalpy environment of the low-density charring ablator considered here was satisfactorily reproduced in a low constant enthalpy test stream specified by the present analysis.

A comparison between calculated and measured char thickness and material degraded thickness for each of the low-density material specimens is shown in Table III. The results predicted by the present analysis are in poor agreement with the test results. The agreement between measured and calculated material degraded thickness is not as bad as that between measured and calculated char thicknesses.

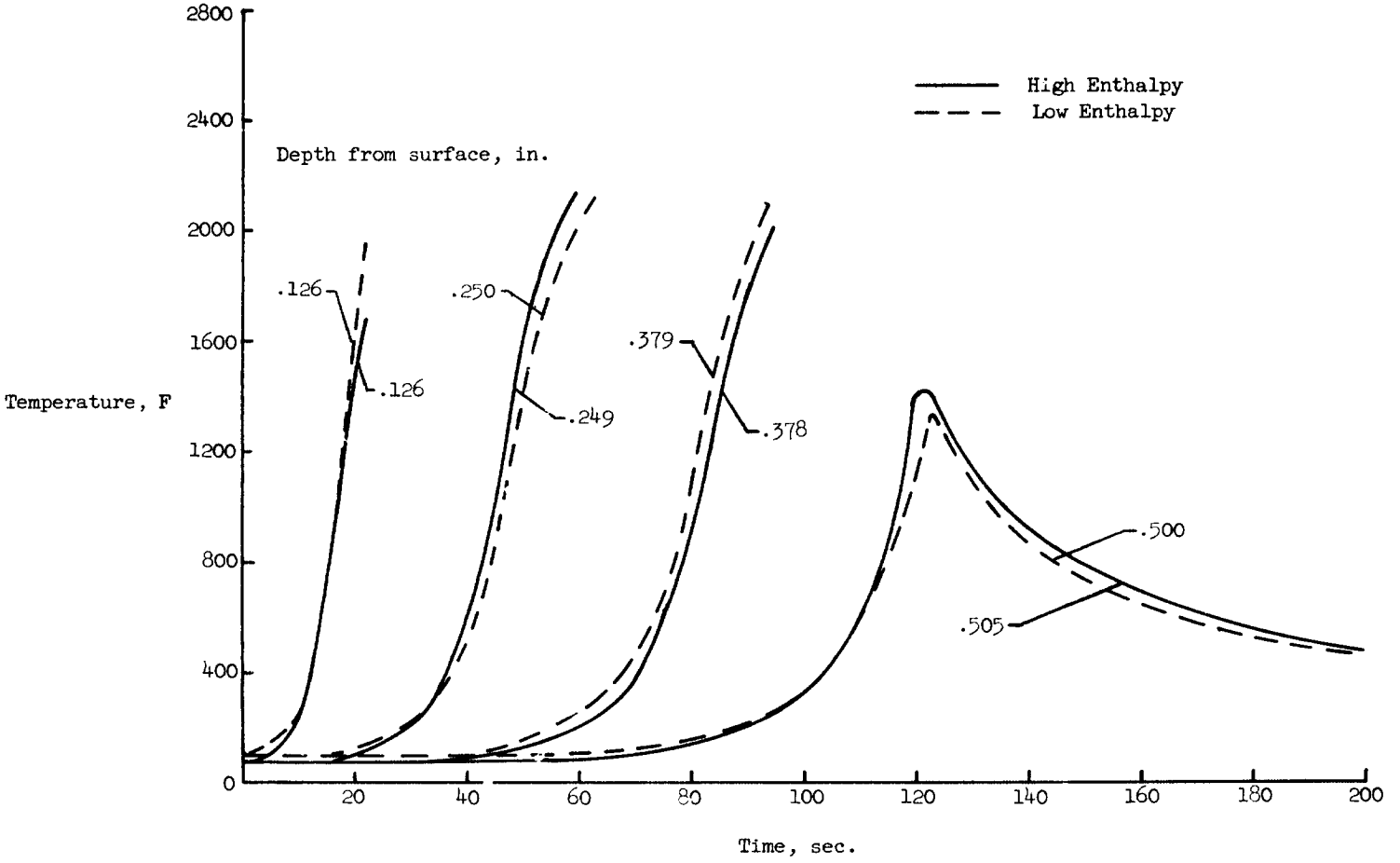

Figure 9.- Internal temperature histories for low-density phenolic nylon specimens.

TABLE III.- COMPARISON OF CALCULATED AND MEASURED TEST DATA

Specimen No.	Test data		Present analysis		Reference 15	
	Char thickness, in.	Material degraded, in.	Char thickness, in.	Material degraded, in.	Char thickness, in.	Material degraded, in.
LD-15	0.13	0.17	0.172	0.204	0.135	0.18
14	0.14	0.17	0.172	0.204	0.145	0.18
13	0.2	0.31	0.278	0.344	0.185	0.275
7	0.2	0.31	0.278	0.344	0.18	0.29
16	0.22	0.41	0.315	0.480	0.215	0.375
5	0.23	0.42	0.315	0.480	0.21	0.385
3	0.23	0.52	0.420	0.546	0.249	0.481
1	0.21	0.49	0.420	0.546	0.242	0.494
HD-10	0.07	0.08	0.078	0.099		
9	0.08	0.10	0.078	0.099		
8	0.12	0.17	0.129	0.173		
7	0.12	0.18	0.129	0.173		
13	0.16	0.23	0.165	0.206		
11	0.17	0.25	0.165	0.206		
3	0.18	0.33	0.196	0.294		
6	0.2	0.35	0.196	0.294		

These differences may be accounted for in the following manner. In the present analysis it is assumed that the heating rate is constant over the time period. Figure 7 shows that the specimen geometry approaches a hemisphere, with time, resulting in an increase in heating with time. This increase would cause a decrease in char thickness due to an increase in surface recession.

Another phenomenon present in these tests that was not accounted for in the analysis is the lateral flow of internal gases. This effect is discussed in detail in Reference 15. Also, Reference 15 presents test data, for a low-density phenolic nylon material similar to the material in the present study, that were successfully matched only when the lateral flow of internal gas was considered. Briefly, this lateral flow results in a reduction in mass transfer into the boundary layer caused by the lateral flow of pyrolysis gases and the inflow of gases at the surface. This lateral flow results from a combination of char permeability, external pressure field, and the ratio of char thickness to specimen body radius. Incorporating the lateral flow analysis of Reference 15 into the transient ablation analysis of Reference 3 and applying this to the present tests gives the indicated results shown in Table III. In addition, it was found necessary to reduce the char density from 16 lb/ft^3 to 12 lb/ft^3 to obtain the results in Table III. A measured char density of 16 lb/ft^3 was used to determine the nominal test conditions, however, a char density of 12 lb/ft^3, which was also measured, is reported in Reference 10 for this material. These chars were formed under different conditions. As can be seen, the agreement

between calculated and measured char thickness and thickness of material degraded is satisfactory. Calculations indicated that the internal flow phenomenon effected the test results by about the same magnitude in both high and low enthalpy environments, see Table III.

High-Density Phenolic Nylon Specimens

Photographs of the tested specimens are shown in Figure 10. For each specimen tested at high enthalpy there is a corresponding specimen tested at low enthalpy. The total recession, char thickness, and thickness of material degraded for each specimen are given in Table II and the data are plotted in Figure 11. Also shown in Table II are the required and actual test conditions for the low enthalpy tests.

From a visual comparison of the paired specimens in Figure 10, it is seen that the char surface, thickness, and structure are similar. As was previously mentioned, the cracked pattern present on all the char surface is believed to occur during cooling. The source of the sunburst pattern on the specimen tested for 30 seconds at high enthalpy is not known.

Figure 11 shows the pyrolysis zone and outer surface location histories for the high density phenolic nylon specimens. Again the differences are within the accuracy of the measurements. The agreement is very good, indicating satisfactory reproduction of the transient surface and pyrolysis zone behavior.

Figure 12 shows internal temperature histories for models tested at the low and high enthalpy conditions. The agreement is satisfactory.

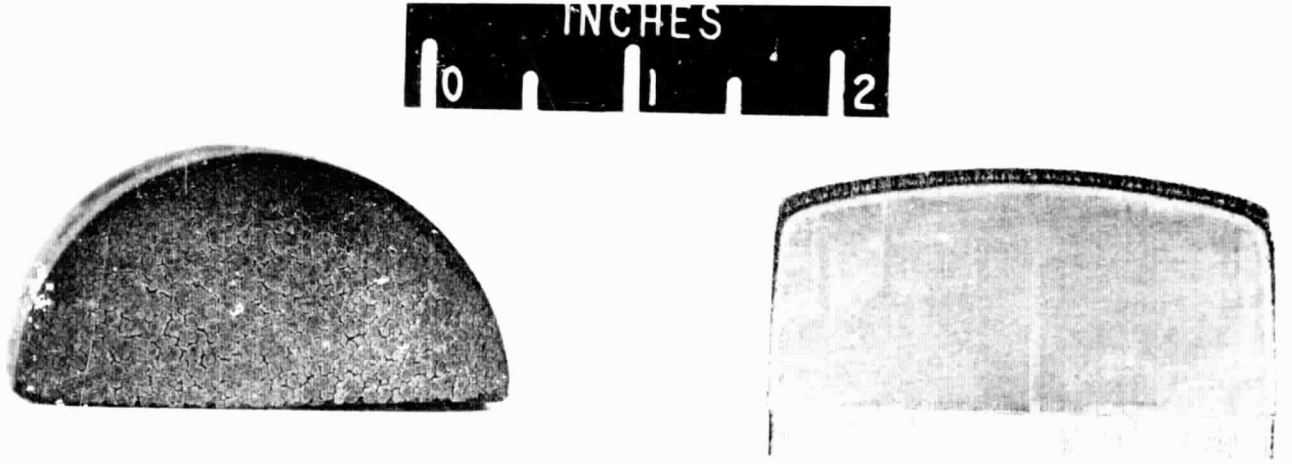

(a) Specimen HD-10 tested 30 seconds at high enthalpy.

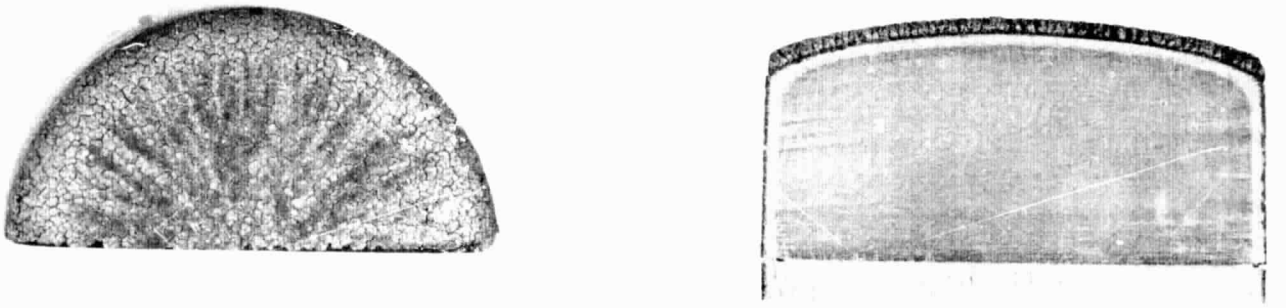

(b) Specimen HD-9 tested 30 seconds at low enthalpy.

Figure 10.- High-density pehnolic nylon specimens after testing.

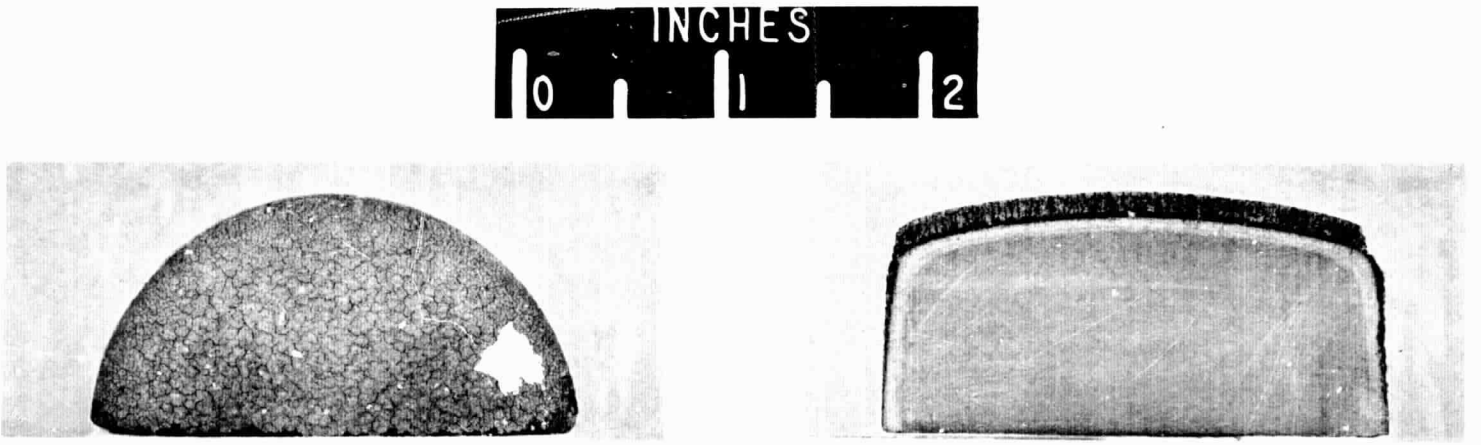

(c) Specimen HD-8 tested 60 seconds at high enthalpy.

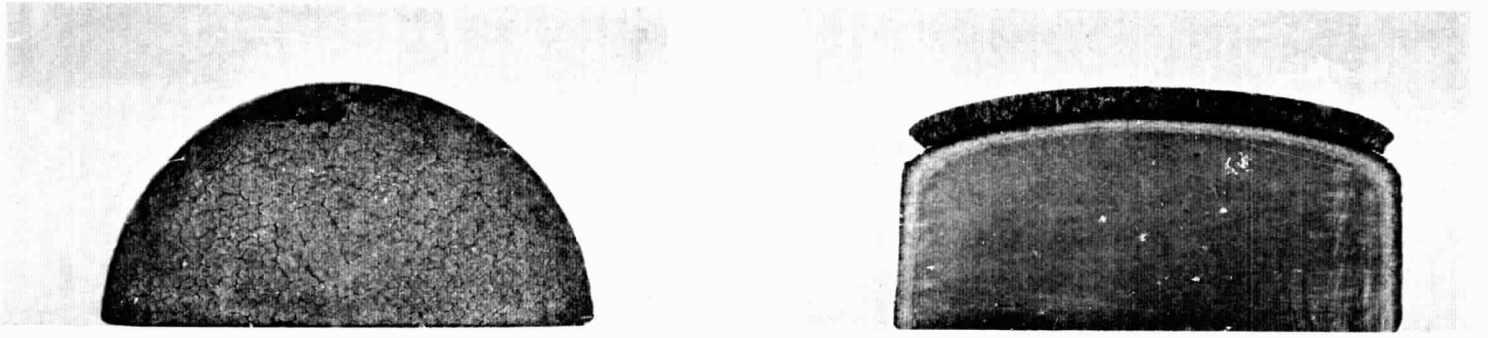

(d) Specimen HD-7 tested 60 seconds at low enthalpy.

Figure 10.- Continued.

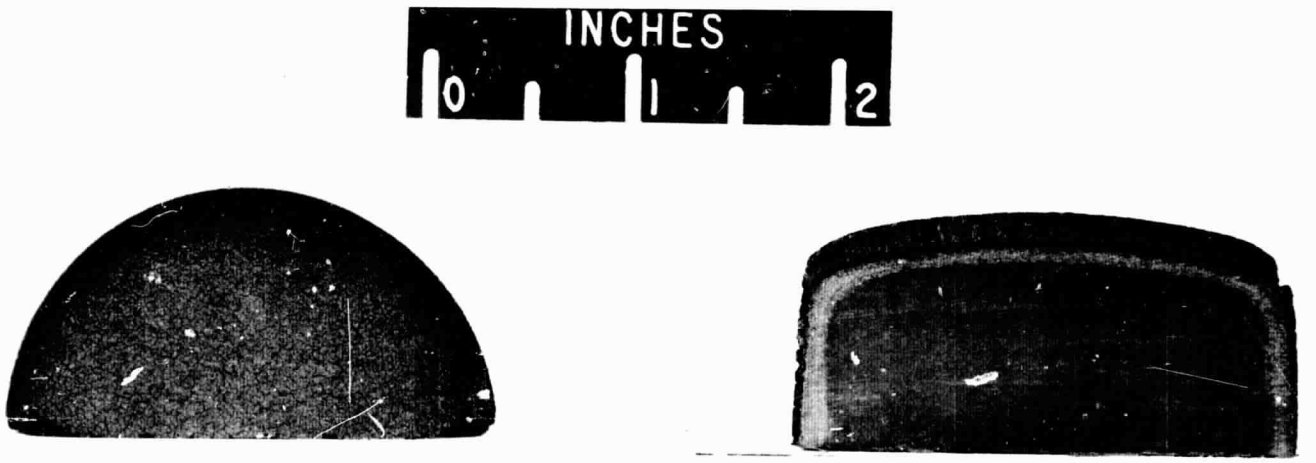

(e) Specimen HD-13 tested 90 seconds at high enthalpy.

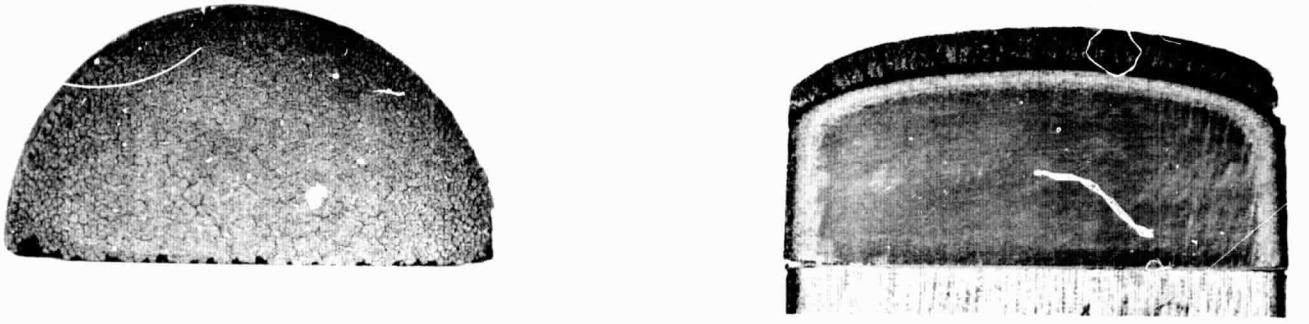

(f) Specimen HD-11 tested 90 seconds at low enthalpy.

Figure 10.- Continued.

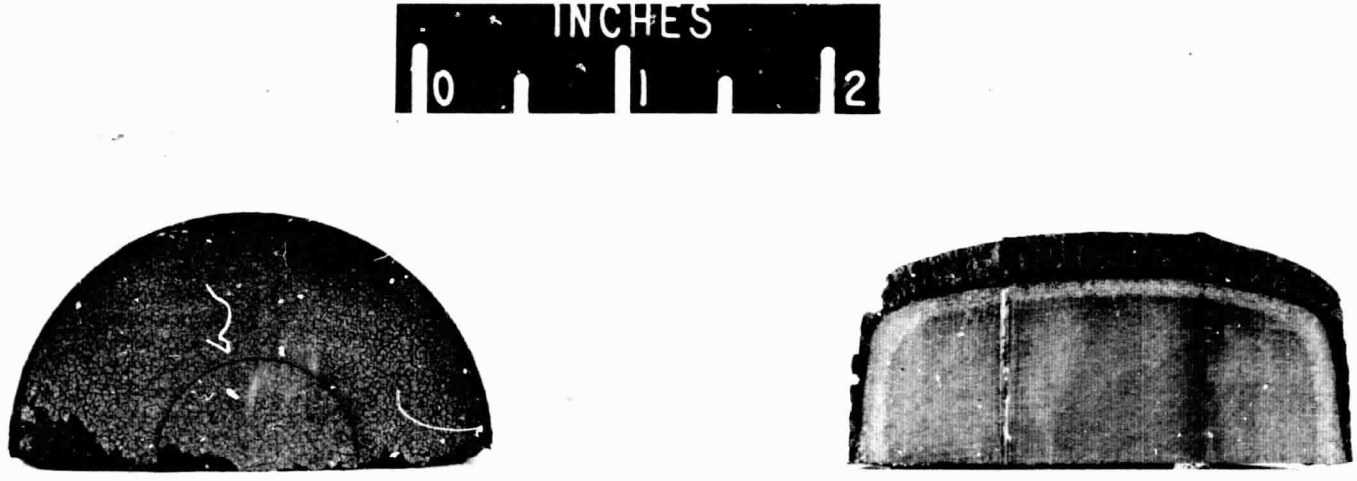

(g) Specimen HD-3 tested 130 seconds at high enthalpy.

(h) Specimen HD-6 tested 120 seconds at low enthalpy.

Figure 10.- Concluded.

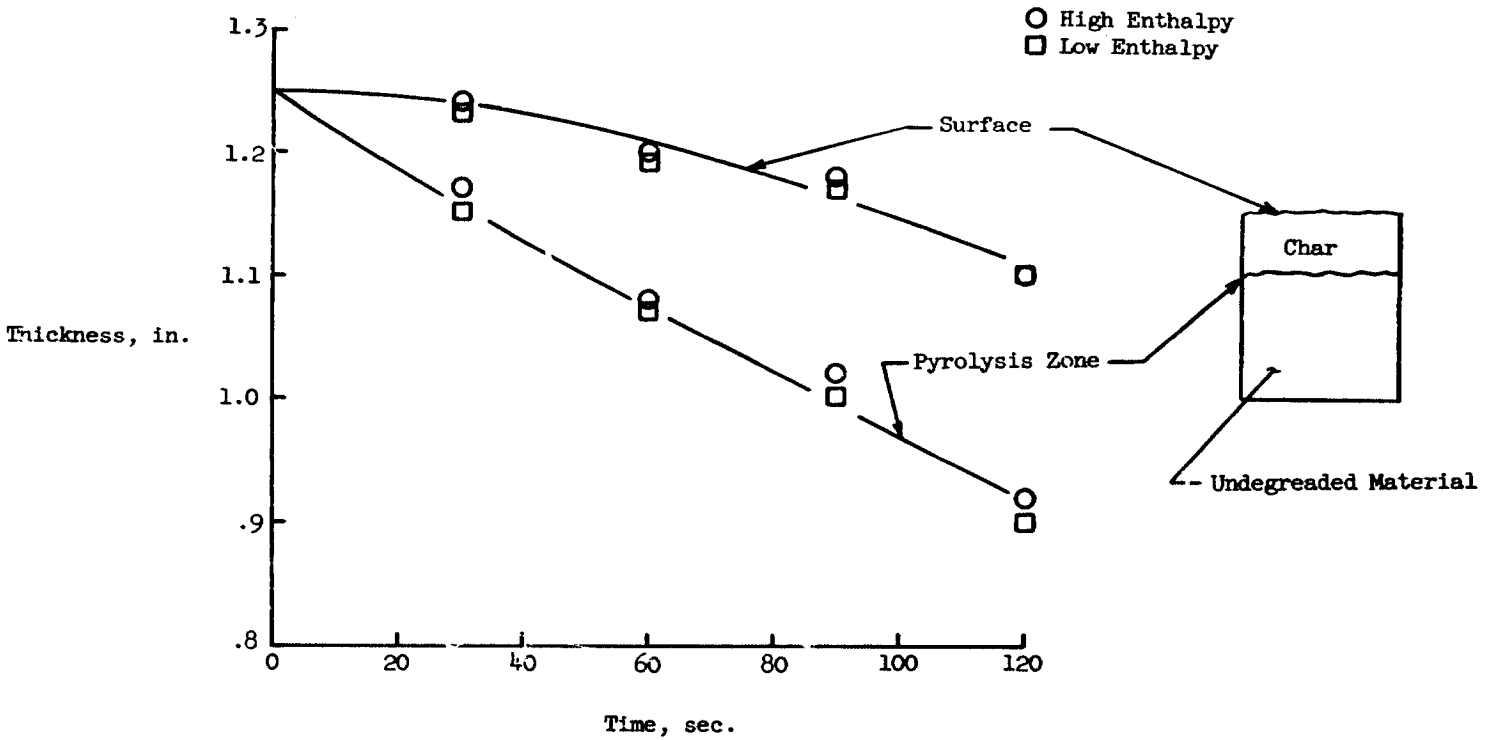

Figure 11.- Surface and interface location histories for high-density phenolic nylon.

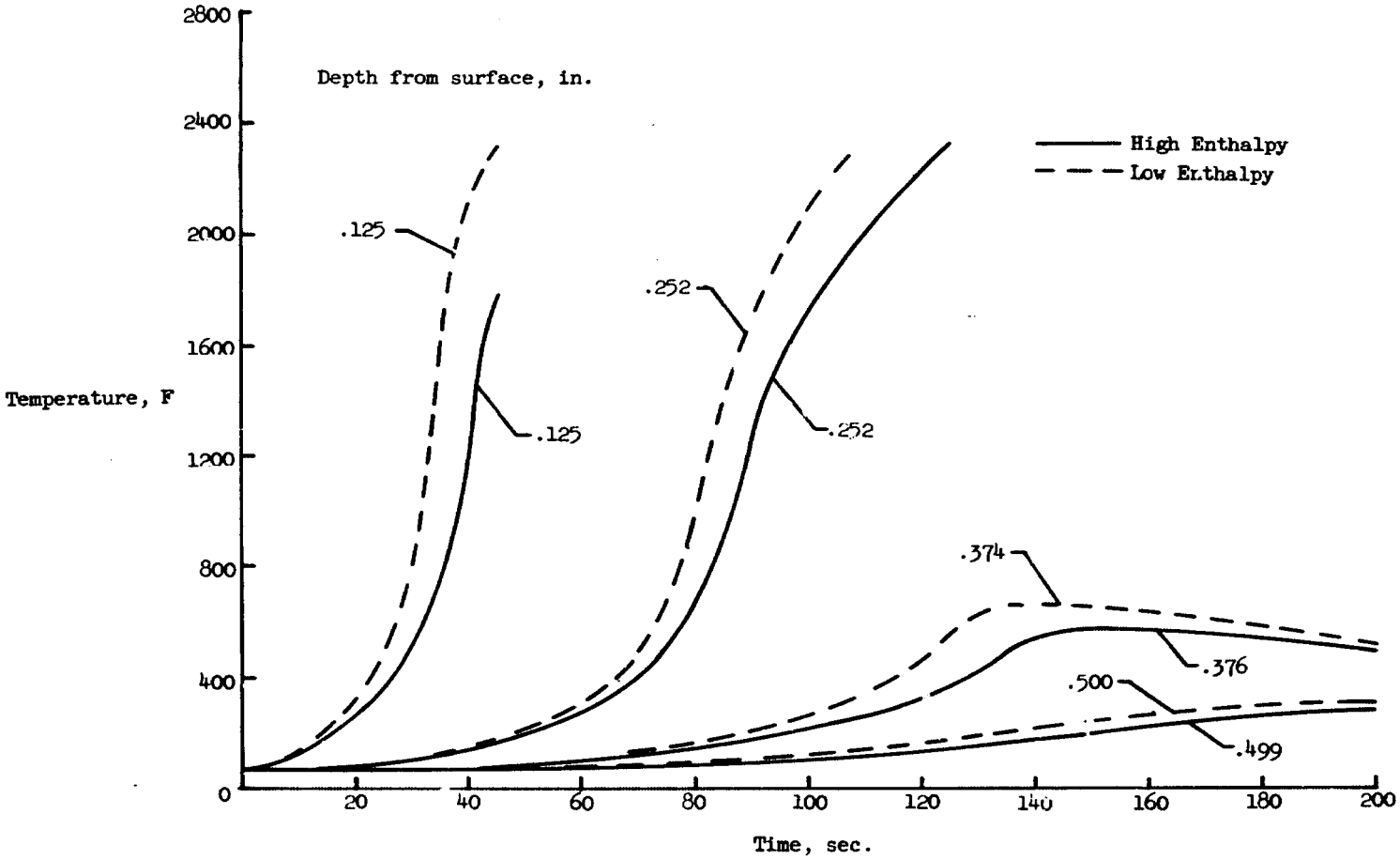

Figure 12.- Internal temperature histories for high-density phenolic nylon.

The differences may be attributed to the heating rate experienced by the specimen tested at low enthalpy which was higher than that required for simulation.

An examination of the data presented in Figures 10, 11, and 12 shows that the transient ablation performance in a high enthalpy environment of the high-density charring ablator considered here was satisfactorily reproduced in a low enthalpy test stream specified by the present analysis.

A comparison between measured char thickness and material degraded thickness and the corresponding thicknesses computed by the present analysis for each specimen is shown in Table III. The agreement is satisfactory. Hence, it is assumed that the lateral flow of internal gases present in the low-density phenolic nylon specimens was not present in this material for these tests. Under some test conditions, however, the lateral flow of internal gases may be important for this material.

In summary, relationships have been obtained that determine the heat input (eq. (6)) and the stream oxygen content (eq. (14)) required in a low constant enthalpy environment to simulate the ablation performance of a charring ablator in a high constant enthalpy environment. Two types of phenolic nylon ablation materials have been tested in environments related by equations (6) and (14). A comparison of these test data (the char recession, char thickness, thickness of material degraded, internal temperatures histories, and physical appearance) will indicate if satisfactory simulation of the ablation performance can be obtained.

A brief comparison of the test data is given in Table IV. The reproducibility at low enthalpy of the char recession, char thickness, and thickness of material degraded measured at high enthalpy, is determined by the percentage difference between these thicknesses at low and high enthalpy. The ratio of the accuracy of the measurement, ±0.01 inch, to the thickness measured is also given in Table IV as the percentage of accuracy. All percentages are based on the thicknesses measured at high enthalpy. It is believed that any significant difference in ablation performance could be discernible by the accuracy used for this study. Table IV, therefore, indicates that the thickness data from these two sets of tests are in good agreement.

Hence, a comparison of the physical appearance and the internal temperature histories, together with the thickness data, indicate that satisfactory simulation of the ablation performance of these two materials was obtained.

Variable Enthalpy Heating

The present analysis applies to the simulation of the performance of a char forming ablator subjected to high constant enthalpy heating in a low constant enthalpy heating environment. The preceding test results indicate that this analysis can be satisfactorily used to obtain good simulation. In this section a method will be outlined that may be used to simulate the performance of a material subjected to high, variable enthalpy heating, typical of entry into a planetary atmosphere, in a constant enthalpy heating environment.

TABLE IV.- COMPARISON OF THICKNESS DATA

Time, sec	Low-density material				High-density material			
	30	60	90	120	30	60	90	120
Recession,								
Percent difference	25	0	0	3	100	20	14	7
Percent accuracy	25	8	5	3	100	20	14	7
Char thickness,								
Percent difference	8	0	5	8	14	0	6	5
Percent accuracy	8	5	5	4	14	8	6	5
Material degraded,								
Percent difference	0	0	2	6	24	6	8	6
Percent accuracy	6	3	2	2	12	6	4	3

Figure 13 shows a typical enthalpy and cold-wall stagnation heating rate history for a manned lifting-body vehicle entering the earth's atmosphere. To apply the approximate ablation analysis of Reference 7, a constant enthalpy heating condition must exist. Therefore, an approximation of the enthalpy history in Figure 13 is needed. To approximate constant enthalpy heating, a variable enthalpy heating trajectory, such as the one in Figure 13, may be divided into a number of steps or intervals over which the enthalpy may be considered constant. A typical step is indicated in Figure 13 between 500 and 600 seconds. It may, therefore, require a large number of steps to approximate the enthalpy history.

Applying the approximate ablation analysis to the approximated enthalpy history and undisturbed heating history, the char weight formed during each step is obtained from equations (6), (7), and (8). The total weight of material degraded during a step is obtained from equation (10). The heat input for a given step is obtained by integrating the heating rate over that step (Fig. 13). The initial weights used in equations (6) and (10) are the final weights from the previous step.

This approximation to the enthalpy history allows the present analysis to be used to simulate the performance of a charring ablator subjected to a varying enthalpy heating environment in a constant enthalpy environment. The required oxygen concentration of the test stream for simulation during a given step is obtained from equation (14). Since the char weight and the extremum char weight are the same in flight

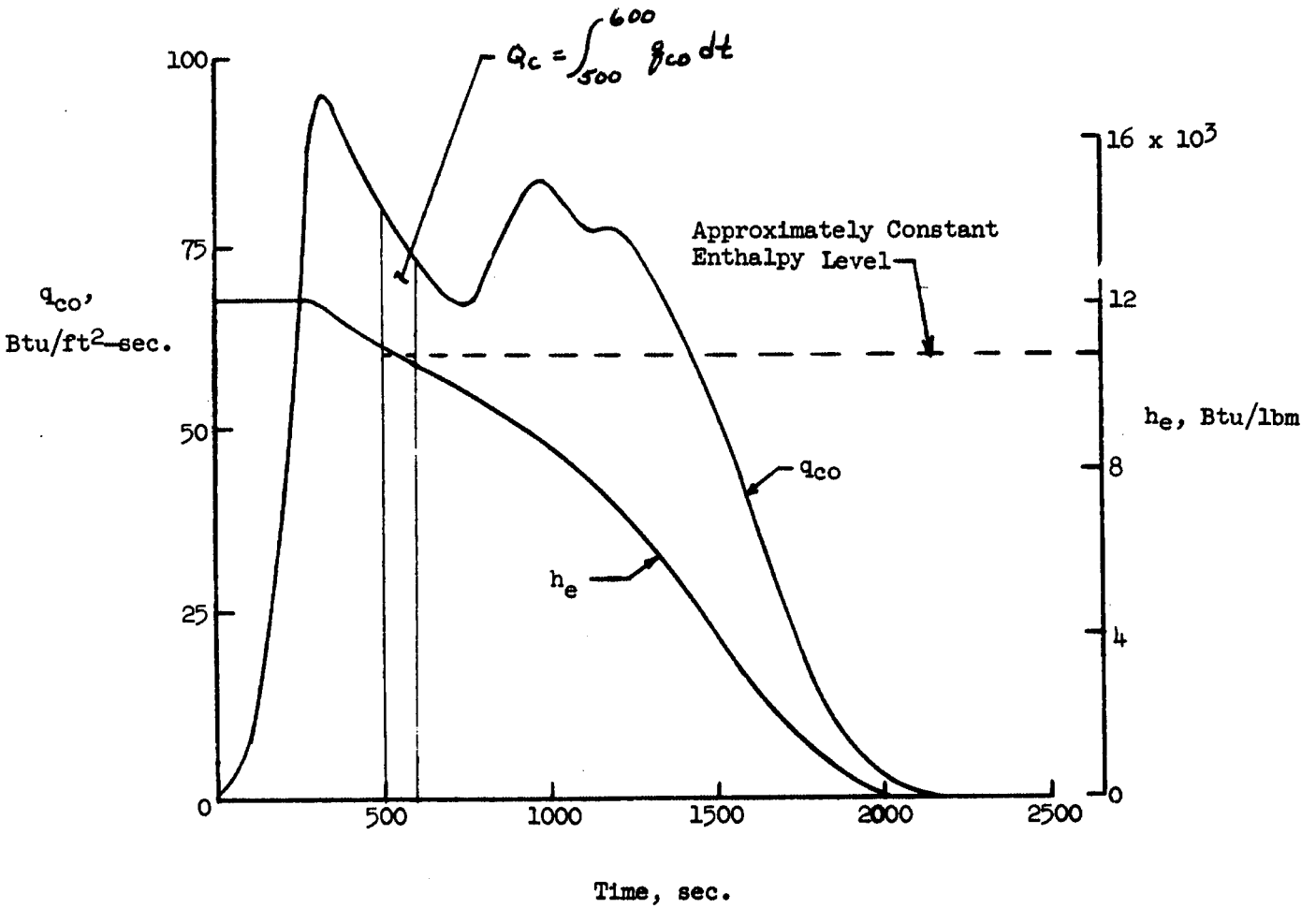

Figure 13.- Enthalpy and stagnation cold-wall heating rate histories experienced by typical manned lifting-body entry vehicle.

and test for each step, the magnitudes of W_c and $W_{c,m}$ are obtained from equations (6), (7), and (8) using the approximated flight conditions. The test heat input is found by scaling the flight heat input through equation (6). The test time for a step may be obtained from equation (16). Since the values of C_e, Q_c, and t obtained with equations (6), (14), and (16) apply to only one step, the above process must be repeated for each step using the final weights from the previous step as the initial weights for the next step. Therefore, the test required to simulate the ablation performance at varying enthalpy will consist of a series of steps of different C_e, Q_c, and t at constant enthalpy.

CHAPTER VII

CONCLUDING REMARKS

The conditions under which the performance of a charring ablator in a high enthalpy environment can be simulated in a low enthalpy environment have been examined. An approximate ablation analysis has been used to obtain quantitative relationships between a low enthalpy heating environment and a high enthalpy heating environment to obtain the same ablation performance of a charring ablator in both environments.

Tests were made to determine the ablation performance of a low-density phenolic nylon material and a high-density phenolic material in air at a constant high enthalpy heating condition. Identical specimens of each material were also tested in a constant low enthalpy test stream related to the high enthalpy environment by the aforementioned relationships. These tests indicated that satisfactory simulation of the ablation performance of these two materials was obtained.

The low-density phenolic nylon material performance was affected by its high char permeability and external pressure environment. However, the material performance appeared to be affected to the same degree in both high and low enthalpy environments. The high-density phenolic nylon material did not appear to be affected in this way.

The tests presented in this paper indicate that satisfactory simulation was obtained. However, convective heating at constant enthalpy was the only case considered. A method is outlined to extend the present technique to simulate the ablation performance at variable

enthalpy with convective and radiative heating in a constant enthalpy environment with convection only. Simulation of the latter case at constant enthalpy with radiation as the prime source of heat is also discussed.

REFERENCES

1. Chapman, Andrew J.; Effects of Weight, Density, and Heat Load on Thermal-Shielding Performance of Phenolic Nylon. NASA TN D-2196, June 1964.
2. Clark, Ronald K.; Effects of Environmental Performance of Low-Density Silicone-Resin and Phenolic-Nylon Ablation Materials. NASA TN D-2543, January 1965.
3. Swann, R. T., Pittman, C. M., and Smith, J. C.; One-Dimensional Numerical Analysis of the Transient Response of Thermal Protection System. NASA TN D-2976, September 1965.
4. Tompkins, S. S., and Dow, M. B.; Parametric Study of a Low-Density Charring Ablator. NASA TN D-3735, December 1966.
5. Walberg, Gerald D.; Analysis Study of Diffusion-Controlled Char Oxidation and Its Effect On Steady-State Ablation of Plastic Materials. NASA TR-R-242, July 1966.
6. Dow, M. B., and Swann, R. T.; Determination of Effects of Oxidation on Performance of Charring Ablators. NASA TR-R-196, June 1964.
7. Swann, Robert T.; Approximate Analysis of the Performance of Char-Forming Ablators. NASA TR-R-195, June 1964.
8. Swann, R. T., Dow, M. D., and Tompkins, S. S.; Analysis of the Effects of Environmental Conditions on the Performance of Charring Ablators. J. of Spacecraft and Rockets, vol. 3, no. 1, January 1966, pp. 61-67.

9. Stroud, C. W.; A Study of the Chemical Reaction Zone in Charring Ablators During Thermal Degradation. NASA Paper Presented at the Meeting of the American Institute of Chemical Engineers (Dallas, Texas), February 6-9, 1966.

10. Wilson, Gale R. (Compiler); Thermophysical Properties of Six Charring Ablators From 140° to 700°K and Two Charr From 800° to 3000°K. NASA TN D-2991, October 1965.

11. Brewer, William D.; Effects of Thermocouple Wire Size and Configuration in Internal Temperature Measurements in a Charring Ablator. NASA TN D-3812, March 1967.

12. Schaefer, William T., Jr.; Characteristics of Major Active Wind Launch at the Langley Research Center. NASA TM X-1130, July 1965.

13. Fay, J. A., and Riddell, F. R.; Theory of Stagnation Point Heat Transfer in Dissociated Air. J. Aero. Sci., vol. 25, no. 2, February 1958, pp. 73-85, 121.

14. Hansen, C. Frederick; Approximation for the Thermodynamic and Transport Properties of High-Temperature Air. NASA TR-R-50, 1959 (Supersider NACA TN 4150).

15. Bush, H. G., and Dow, M. B.; Multidimensional Gas Flow Through Permeable Char Layers and Its Effect on Ablation. Proposed NASA TR (L6034).

16. Swann, Robert T.; Composite Thermal Protection Systems for Manned Re-Entry Vehicles. ARS J., vol. 32, no. 2, February 1962, pp. 221-226.

17. Beckwith, Ivan E.; Similar Solutions for the Compressible Boundary Layer on a Yawed Cylinder With Transpiration Cooling. NASA TR-R-42, 1959.

APPENDIX A

ASSUMPTIONS

A number of simplifying assumptions must be made if approximate analytical relations governing the performance of charring ablators are to be obtained. The assumptions used in the analysis on which the present paper is based are:

1. The specific heat of the char is neglected. This assumption reduces the problem from a transient to a quasi-steady-state condition. Calculations based on this assumption are compared to numerical solutions which include specific heat effects in Reference 16 and the agreement is satisfactory.

2. The thermal conductivity of the char is assumed to be a function of temperature as follows:

$$k = \frac{k_r(T_s^2 + T_p^2)(T_s + T_p)}{(T_r^2 + T_p^2)(T_r + T_p)}$$

The thermal conductivity of a porous material such as a char layer will increase with increasing temperature because of radiation across the void spaces. Relatively large changes in heating rate are required to obtain significant changes in the surface temperature because the surface reradiation energy at a rate proportional to the fourth power of the temperature. Therefore, by proper selection of the reference temperature, T_r, the error introduced can be minimized.

3. Char removal is assumed to occur only as a result of a diffusion limited oxidation mechanism. This yields a maximum rate at which char can be removed by oxidation, and will be conservative if oxidation is the only mechanism of char removal.

4. The product of combustion is assumed to be carbon monoxide, and all of the heat generated by the reaction is assumed to go into the surface.

5. For moderate mass transfer the reduction in convective heating resulting from mass transfer into the boundary layer is assumed to be directly proportional to the rate of mass transfer (Ref. 3). It is also assumed that the char which is oxidized and the pyrolysis products which are injected into the boundary layer are equally effective in blocking the convective heat input.

6. The Lewis number is assumed to be unity, that is,

$$N_{Le} = \frac{N_{Pr}}{N_{Sc}} = \frac{C_p \rho D}{k} = 1$$

This indicates that the mechanism of oxygen diffusion is the same as heat transfer in the boundary layer. Although the value of the Lewis number is a function of the temperature and the gas being considered, the Lewis number is roughly unity for most gases of interest. Also, Reference 17 indicates that heat transfer at the stagnation point is not sensitive to the effect of dissociation, that is, $N_{Le} = 1$.

APPENDIX B

SIMULATION WITH RADIATIVE HEATING

When radiant heating is the prime heating mode, it is assumed that the gas flow over the surface is used only to provide the required oxidation of the surface, and to remove the gaseous products of pyrolysis. The convective heating is approximately equal to zero, as is the difference between the enthalpy of the stream external to the boundary layer and at the surface. However, the ratio of the heating rate to the enthalpy difference has a definite value which is the heat transfer coefficient.

$$\gamma = \frac{q_{c,net}}{h_e - h_w} \qquad h_e \rightarrow h_w \tag{B-1}$$

The following relations are obtained from Reference 7, using equation (B-1):

$$\frac{dW_c}{dt} = \frac{1 - f}{f} \dot{m}_p - a\gamma \tag{B-2}$$

The heat balance at the surface becomes

$$q_1 + \alpha q_r = \dot{m}_p \Delta h_{eff} \left(\frac{W_c}{\beta} + 1 \right) \tag{B-3}$$

where

$$q_1 = a\gamma\Delta h$$

Combining equations (B-2) and (B-3),

$$\frac{\alpha q_r}{\Delta h_{eff}} + \frac{a\gamma\Delta h}{\Delta h_{eff}} = \left(\frac{dW_c}{dt} + a\gamma\right)\frac{f}{1 - f}\left(\frac{W_c}{\beta} + 1\right) \tag{B-4}$$

The extremum char weight then becomes,

$$W_{c,m} = \beta\left[\left(\frac{1 - f}{f}\right)\left(\frac{\alpha q_r}{a\gamma\Delta h_{eff}} + \frac{\Delta h}{\Delta h_{eff}}\right) - 1\right] \tag{B-5}$$

For the test environment, equations (6), (7b), and (10) become:

$$\frac{W_i - W_c}{W_{c,m}} - \left(1 + \frac{\psi\beta}{W_{c,m}}\right)\ln\left(\frac{1 - \dfrac{W_c}{W_{c,m}}}{1 - \dfrac{W_i}{W_{c,m}}}\right) = \frac{a\gamma t}{(1 + a\eta)W_{c,m}} \tag{B-6}$$

where

$$\psi = 1 + \frac{\eta a\Delta h}{\Delta h_{eff}(1 + a\eta)} \tag{B-7}$$

and

$$W = \frac{W_c - W_i + \left(\dfrac{a}{1 + a\eta}\right)\gamma t}{\dfrac{1 - f + a\eta}{1 + a\eta}} \tag{B-8}$$

Assume that both convective and radiative heating are present in the flight environment. The extremum char weight for the flight environment is given by equation (8). The oxygen concentration in the test stream is determined by equating equations (8) and (B-5),

$$\frac{(C_e)_1}{(C_e)_2} = \frac{\dfrac{(\alpha q_r)_1}{\gamma_1 (h_e - h_w)_2}}{\left[1 + \left(\dfrac{q_r}{q_{co}}\right)\left(1 + \dfrac{a\eta}{1 - f}\right)\right]_2} \tag{B-9}$$

The required radiant heat rate is obtained from the equation

$$(\alpha q_r)_1 = (\alpha q_r)_2 + (q_{co})_2 \left(1 - \frac{h_w}{h_e}\right)_2 \left[1 - (\eta_c \dot{m}_c + \eta_p \dot{m}_p)\frac{h_e}{q_{co}}\right]_2 \tag{B-10}$$

The required test time is related, as before, to the flight time by equation (16).

In summary, to simulate the ablation performance of a charring ablator in a flight environment, in which both convective and radiative heating are present, the required oxygen concentration in a test stream is determined from equation (B-9), the radiant heating rates determined by equation (B-10), and the test time by equation (16). The test stream heat transfer coefficient required for simulation is obtained from equation (B-6) using the flight char weight from equation (6).